- 1 Dynamics, predictability, impacts, and climate change considerations of the catastrophic 2 **Mediterranean Storm Daniel (2023)**
- Emmanouil Flaounas^{1,2}, Stavros Dafis³, Silvio Davolio^{4,5}, Davide Faranda^{6, 7, 8}, Christian Ferrarin⁹, 3
- Katharina Hartmuth¹, Assaf Hochman¹⁰, Aristeidis Koutroulis¹¹, Samira Khodayar¹², Mario Marcello Miglietta^{13,-14}, Florian Pantillon¹⁵, Platon Patlakas^{2,16}, Michael Sprenger¹, Iris Thurnherr¹ 4
- 5

- 8 1. Institute for Atmospheric and Climate Science, ETH Zurich, Zurich, Switzerland
- 9 2. Institute of Oceanography, Hellenic Centre for Marine Research, Athens, Greece
- 10 3. National Observatory of Athens, Institute for Environmental Research and Sustainable
- 11 Development, I. Metaxa & Vas. Paylou, P. Penteli (Lofos Koufou), 15236 Athens, Greece
- 12 4. Dipartimento di Scienze della TerraDepartment of Earth Sciences "Ardito Desio", Universitày di of
- 13 Milano, Milan, Italy
- 14 5. Institute of Atmospheric Sciences and Climate, National Research Council, Bologna, Italy
- 15 6. Laboratoire des Sciences du Climat et de l'Environnement, UMR 8212 CEA-CNRS-UVSQ,
- 16 Université Paris-Saclay & IPSL, CE Saclay l'Orme des Merisiers, 91191 Gif-sur-Yvette, France
- 17 7. London Mathematical Laboratory, 8 Margravine Gardens, London W6 8RH, UK
- 8. LMD/IPSL, ENS, Université PSL, École Polytechnique, Institut Polytechnique de Paris, Sorbonne 18
- 19 Université, CNRS, Paris France
- 20 9. CNR - National Research Council of Italy, ISMAR - Institute of Marine Sciences, Venice, Italy
- 21 10. Fredy and Nadine Herrmann Institute of Earth Sciences, Hebrew University of Jerusalem,
- 22 Edmond Safra Campus, Jerusalem, Israel
- 23 11. School of Chemical and Environmental Engineering, Technical University of Crete, 73100
- 24 Chania, Greece
- 25 12. Mediterranean Centre for Environmental Studies (CEAM), Charles R. Darwin Street, 14 46980
- 26 Paterna, Valencia (Spain)
- 27 13. Institute of Atmospheric Sciences and Climate, National Research Council, Padua, Italy
- 28 14. Department of Geosciences, University of Bari, Bari, Italy
- 29 15. Laboratoire d'Aérologie, Université de Toulouse, CNRS, UPS, IRD, Toulouse, France
- 30 16. Department of Physics, National and Kapodistrian University of Athens, Athens, Greece

31

Abstract

33 34 35

36

37

38

39

In September 2023, Storm Daniel formed in the central Mediterranean Sea as an intense Mediterranean cyclone, causing significant socioeconomic impacts in Greece, including fatalities and severe damage to agricultural infrastructure. Within a few days, it evolved into a tropicallike storm (medicane) that made landfall in Libya, likely becoming, to our knowledge, the most catastrophic and lethal weather event ever documented in the region.

40 This study places Storm Daniel as a centerpiece of the disasters in Greece and Libya. We aim to 41 conduct a comprehensive analysis that links a cyclone system with hazardous weather relevant 42 to extreme precipitation, floods, and significant sea wave activity. In addition, we examine 43 Daniel's predictability in different development stages and draw connections with previous case 44 studies. Finally, given the extreme precipitation produced by Daniel, we place our findings in a

45 climatological context to better understand its implications for numerical weather prediction

46 and climate change attribution.

47 Daniel initially developed like any other intense Mediterranean cyclone, including medicanes, 48 due to upper tropospheric forcing followed by Rossby wave breaking. At this stage, it produced 49 significant socioeconomic impacts in Greece, even in areas far from its center. As it intensified 50 and attained troincludipical-like characteristics, it peaked after landfall in Libya, where its 51 socioeconomic impacts were the most severe. The cyclone's formation had low predictability 52 even at short lead times (around four days), while the landfall in Libya was more predictable 53 within the same lead time. Our analysis of impacts highlights that numerical weather prediction

54 <u>models can capture the extreme character of precipitation and flooding in both Greece and</u> 55 Libya, providing crucial information on the expected severity of imminent flood events.

We also examine moisture sources contributing to extreme precipitation. Our findings indicate that large-scale atmospheric circulation was the primary driver, but, as Daniel matured, it drew substantial water vapor from local maritime areas within the Mediterranean. Daniel produced extreme precipitation amounts in a climatological context, fueled by a warmer Mediterranean Sea and atmosphere. Our analysis supports interpreting its impacts as characteristic of human-driven climate change but also highlights the exceptionality of this cyclone, especially in its medicane phase, which complicates the comparison with other cyclones.

In September 2023, storm Daniel formed in the centre of the Mediterranean Sea as an intense Mediterranean cyclone. Its formation was accompanied by significant socioeconomic impacts in Greece including several fatalities and severe damages to agricultural infrastructures. Within a few days, the cyclone evolved into a tropical-like storm, i.e., medicane, that made landfall in Libya, probably marking the most catastrophic and lethal weather event that was ever documented in the region. In this study, we place storm Daniel as the centrepiece of the catastrophic events in Greece and Libya. We thus consider that there is a direct link between the atmospheric processes that turned Daniel into a catastrophic storm and the actual socioeconomic impacts that a single weather system has produced in the two countries. We perform a holistic analysis that articulates between atmospheric dynamics, precipitation extremes, and quantification of impacts, i.e., floods and sea state. This is done by taking into account the predictability of Daniel at weather scales and the attribution of impacts to climate change.

Our results show that Daniel initially formed like any other intense Mediterranean cyclone. At this stage, the cyclone produced significant socioeconomic impacts on Greece, in an area far from the cyclone centre. In later times, Daniel attained tropical-like characteristics while gradually reaching its maximum intensity. Impacts over Libya coincided with the cyclone's landfall at its maturity stage. The predictability of the cyclone formation was rather low even in relatively short lead times -of the order of four days- while higher prediction skill was found when addressing the landfall in Libya for the same lead times. Our analysis of impacts shows the adequate capacity of numerical weather forecasting to capture the extremeness of precipitation amounts and floodings in Greece and Libya. Therefore, state-of-the-art numerical weather prediction has provided information on the severity of the imminent flood events.

We also analyse the moisture sources contributing to extreme precipitation. Results show that moisture sources were majorly driven by large-scale atmospheric circulation, while in maturity, Daniel drew substantial amounts of water vapor from local maritime areas within the Mediterranean Sea. In a climatological context, Daniel was indeed shown to produce extreme precipitation amounts, and our analysis allows us to interpret Daniel's impacts as an event whose characteristics can be ascribed to human-driven climate change.

1. Introduction

In September 2023, a low-pressure system developed within the central Mediterranean Sea, close to Greece. Due to the expected severity of the event, on 4 September 2023, the Hellenic National Meteorological Service named the storm 'Daniel-'. Within a few days, Daniel evolved into a deep cyclone that propagated southwards, making landfall at the coast of Libya (Fig. 1a). Daniel led to substantial, unprecedented socio-economic impacts in the Central-Eastern Mediterranean from 4 to 11 September 2023, all attributed to the same weather system.

In the cyclogenesis stage, on 5 September 2023, the weather station network of the National Observatory of Athens in Greece (NOAAN; Lagouvardos et al., 2017) measured more than 750 mm of accumulated daily rainfall in the eastern parts of the Thessaly region (flooded areas are shown in cyan colours in Fig. 1b) and up to 1235 mm within four days. The eastern parts of Greece experienced flooding (Fig. 1b) that led to 17 fatalities, the loss of 25% of Greece's annual agricultural production,

and the destruction of the local road network. About five days later, on 10 September 2023, the cyclone made landfall near Benghazi, Libya. As a result, northeastern Libya's population of 884,000 people has been affected directly in five provinces by the collapse of two dams. About 30% of the city of Derna was flooded (Fig. 1c), and almost 900 buildings were destroyed, including road damagedamages to roads and other infrastructure in the area (OCHA 2023, UNICEF 2023). According to the DTM update (IOM 2023), over 5,000 people were presumed dead, 3,922 deaths were registered in hospitals, 10,000 people were declared missing by the Libyan government and Red Crescent Society, while at least 30,000 people were recognized as internally displaced (UNICEF 2023, IOM 2023) in the Derna area. Extensive damage affectedwas shown to critical infrastructure such as hospitals and drinking water supply systems. Many roads were rendered impassable, making it difficult for humanitarian aid and supplies to get through. At least \$10 million budget was allocated from the UN Central Emergency Response Fund to scale up intervention in response to the Libya disaster, and almost 72 million were requested to cope with the most urgent needs of around 250,000 people (OCHA 2023) just for the first three months after the flooding.

About five days later, on 10 September 2023, the cyclone made landfall near Benghazi, Libya. Consequent flooding caused more than 4,000 fatalities, thousands of missing persons, and overwhelming damages, which were aggravated among other reasons by the collapse of city dams. Overall, more than 1150 km² and 1010 km² were flooded in Greece (He et al., 2024) and Libya (Qiu et al., 2023), respectively, including the densely populated city of Derna, Libya (Fig. 1c).

Daniel was an intense cyclone, preceded by Rossby wave breaking, forming an omega blocking configuration (Couto et al., 2024), over the Atlanticand the consequent intrusion of an upper-level trough. This scenario, as it is commonly observed beforeprior to the formation of intense Mediterranean cyclones, including medicanesis typically expected to occurs in the Mediterranean basin (Raveh-Rubin and Flaounas, 2017). From the perspective of atmospheric dynamics, upper tropospheric systems are often precursors of Mediterranean cyclogenesis. Indeed, troughs and cut-off lows correspond to stratospheric air intrusions that impose significantly high potential vorticity (PV) anomalies and thus trigger baroclinic instability (Flaounas et al., 2022). While the formation of Mediterranean cyclones is almost entirely dependent on baroclinic instability, the development and intensification of a cyclone into a deep low-pressure system is also a function of diabatic processes. More precisely, latent heat release close to the cyclone centre, mainly due to convection, is a source of positive PV anomalies at low levels, eventually translating into enhanced cyclonic circulation. Therefore, baroclinic instability and latent heat release are cyclone development's main forcings. Both processes are modulating factors of cyclones' intensification from the cyclogenesis stage until maturity, i.e., when the cyclone reaches its minimum pressure at the centre. A complete review of Mediterranean cyclone dynamics is available by Flaounas et al. (2022), while a recent thorough analysis of the dynamics of another intense cyclone in the central-eastern Mediterranean (Ianos, 2020) is provided by Pantillon et al. (2024).

As an environmental hazard, cyclones may produce heavy precipitation from the stage of genesis until their lysis, close to their centres but also in remote areas due to <u>localized</u>-localised convective cells (Raveh-Rubin and Wernli, 2016), warm conveyor belts and frontal structures (Pfahl et al., 2012; Flaounas et al., 2018). Regardless of whether precipitation is stratiform or convective, the large-scale atmospheric circulation is essential for transporting water vapour toward the Mediterranean and thus "feeding" the cyclone-induced precipitation (Hochman et al., 2024). Indeed, the Mediterranean basin is composed of a relatively closed sea surrounded by high mountains. Consequently, Mediterranean cyclones have fewer water sources than their counterparts in the storm tracks—over the open oceans. In these regards, large-scale ventilation of water vapour from the Atlantic Ocean and other remote regions towards the Mediterranean has been shown in numerous cases to enhance heavy precipitation, together with local evaporation due to cyclone-induced high wind speeds (Duffourg and Ducrocq, 2011; Flaounas et al., 2019; Khodayar et al., 2021; Sioni et al., 2023). Hence, identifying and quantifying the contribution of water sources to heavy precipitation is crucial for understanding socioeconomic impacts in the Mediterranean (Hochman et al., 2022a).

In a climatological context, Mediterranean cyclones produce most of the wind and precipitation extremes in the region (Nissen et al., 2010; Flaounas et al., 2015; Hochman et al., 2022b). Therefore, cyclones play a central role in the compoundness of high-impact weather events (Catto and Dowdy, 2021; Rousseau-Rizzi et al., 2023; Portal et al., 2024), also considering that landfalling systems additionally produce storm surges and significant high waves (Patlakas et al., 2021; Ferrarin et al., 2023a; Ferrarin et al., 2023b;). Especially in the case of precipitation, recent results have shown that intense water vapour transport and PV streamers, as a proxy for Rossby-wave breaking, are two of the main features that lead to extreme Mediterranean events (de Vries, 2021; Hochman et al., 2023). Both of these large-scale atmospheric features favour the development of cyclones into deep, low-pressure systems (e.g., Davolio et al., 2020). Thus, their understanding is crucial for predicting socio-economic impacts on weather and climate scales.

Future trends in cyclone-induced hazards in the Mediterranean are mainly quantified through downscaling experiments (e.g., Reale et al., 2022) or statistical-deterministic methods that generate synthetic tracks (e.g., Romero and Emanuel, 2017). Nevertheless, additional investigation is needed to assess the role of climate change in the intensification of storms that occur in the current climate. While attributing extreme events, such as medicanes and high-impact extratropical storms, is a rather trickydifficult task, recent studies based on analogues have suggested that several recent storms are more intense than expected in the absence of climate change (Faranda et al., 2022, 2023). Further investigation of this critical topic requires a case-to-case approach to take into account the particularities of each storm and to acquire a more holistic understanding of the specific processes related to acquire a more holistic understanding of the specific processes that relate to cyclone intensity that are also affected by climate change.

When a high-impact weather event occurs, it encompasses multiple interconnected aspects often studied separately. First, understanding the event's dynamics and physical processes is crucial for assessing short-term forecasting and climate change implications. Second, the associated hazards—such as floods and windstorms—must be assessed concerning the specific conditions of the affected areas. This also raises questions about hazard predictability. Lastly, the event's severity must be placed within a climatological context to determine whether it produced extreme weather conditions and to attribute its intensity to climate change. Despite their interdependence, all these aspects of a specific weather event are rarely examined through an integrated approach. Our motivation is thus to apply a comprehensive framework, using Storm Daniel as the centerpiece of the September impacts in the eastern Mediterranean, and to provide an interdisciplinary assessment of the event (Shirzaei et al., 2025). The substantial socio-economic damages of storm Daniel in well-distinct locations call for further investigation into the predictability of the cyclone at different weather timescales and its placement in the context of climate change. In this study, we rely on the underlying processes of cyclone dynamics as the factor directly responsible for the socio-economic impacts of Daniel, and In particular, we mainly aim to address the following four questions:

- [1.] How did cyclone development stages relate to flooding in Greece and —Libya?
- [2.] How reliable and accurate <u>werewas</u> numerical <u>models for predicting</u> weather <u>conditions and river discharges</u> <u>prediction models of in relation to imminent hazards at different lead times?</u>
- [3.] <u>Can numerical weather prediction models adequately simulate climate extremes? Arenumerical weather models adequate for the prediction of climate extremes?</u>
- 1.[4.] Can we attribute <u>Storm</u> Daniel to climate change?

The following section describes the datasets and methods, while section 3 briefly describes the storm dynamics. Section 4 analyses Stormstorm Daniel's predictability, and section 5 is devoted to Daniel's attribution to climate change.

2. Datasets and methods

2.1 Datasets

To analyze the evolution of the cyclone and assess its predictability, we use the operational analysis and the ensemble prediction system (EPS) products of the European Centre for Medium-Range Weather Forecasts (ECMWF). Since the last model upgrade at ECMWF (Cycle 48r1), operational analysis and medium-range ensemble forecast data have been available at a grid spacing of about 9 km. The increase in horizontal resolution and improvements in the data-assimilation system resulted in substantial improvements in skill (ECMWF Newsletter, 176, 2023). The EPS comprises 50 members, initialized with a perturbed analysis using slightly altered model physics-comprises 50 members, initialized with a perturbed analysis and using slightly altered model physics, and one control forecast. This probabilistic forecasting system has been designed to provide a range of possible weather conditions up to 15 days ahead, providing an estimation of predictability. Finally, to assess Daniel's climatological aspects, we used ERA5 reanalysis (Hersbach et al., 2020) with hourly atmospheric fields at a 0.25-degree0.25 degrees grid spacing.

We used river discharge data from the Global Flood Awareness System (GloFAS; Grimaldi et al., 2022) to investigate the hydrological impacts of Daniel across Greece and Libya-. GloFAS is an integral component of the Copernicus Emergency Management Service (CEMS), focusing on operational flood forecasting globally. It integrates the open-source LISFLOOD hydrological model with ERA5 meteorological reanalysis data, interpolated to align with GloFAS's resolution (0.05° for version 4.0), and produced with a daily frequencytemporal resolution. This dataset encompasses historical discharge records crucial in establishing the discharge climatology from 1993 to 2023. We employed the European Flood Awareness System (EFAS) data to assess the flood forecast potential. The EFAS system utilises the open-source LISFLOOD hydrological model, calibrated to a refined spatial resolution of approximately 1.5 km at European latitudes. Forecasts are generated twice per day, based on initializations at 00 and 12 UTC, and extend lead times from 5 to 15 days to capture a broad spectrum of potential weather conditions impacting river discharge volumes. These forecasts incorporate data from the 51 ECMWF EPS members, the Deutsches Wetter Dienst (DWD) highresolution forecasts, and the COSMO Local Ensemble Prediction System (COSMO-LEPS) with 20 ensemble members, ensuring a comprehensive analysis of the forecast potential. For this study, we used the EFAS model forecasts driven by the 51 ensemble members of the ECMWF EPS.

Finally, to evaluate Daniel's marine and coastal impacts, we <u>analyzedanalysed</u> the wave results of the Mediterranean Sea Waves Analysis and Forecast (Korres et al., 2023) available via the Copernicus Marine Service (CMEMS). We also determined the wave climatology by <u>analyzinganalysing</u> the Mediterranean Sea wave reanalysis available via CMEMS (1993-2021; Korres et al., 2021).

2.2 Methods

2.2.1 Object diagnostics

We identify two-dimensional objects of extreme precipitation to assess the predictability of major impacts in the EPS forecasts. These objects are defined separately for each member of the EPS as neighbouring grid points where daily <u>precipitation valuesvalues of precipitation and wind speed</u> exceed the 99th percentile in the ERA5 climatology (1990-2020). With these objects, we define the probability of the EPS to forecast extreme weather due to Daniel. Similarly, we define the probability of a cyclone occurrence in <u>the EPS</u> by identifying cyclone masks in each ensemble member as the outermost mean sea level pressure (MSLP) contour that delimits a surface smaller than that of a circular disc with a radius of 200 km.

2.2.2 Air parcel trajectories and moisture source diagnostic

Ten-day air parcel backward trajectories are calculated_<u>from a 30 km horizontal grid</u>-every 20 hPa between 1000 and 300 hPa <u>from starting locations on a regular latitude-longitude grid with a 30 km grid spacing</u> within boxes over Greece and Libya (as shown in Fig. 1a) using the LAGRANTO tool (Wernli and Davies, 1997; Sprenger and Wernli, 2015). We calculated two sets of backward trajectories: (i) the first concerns <u>S</u>storm Daniel, where trajectories started every 6 hours on 5 September 2023 and 11 September 2023 from the Greece and Libya box<u>es</u>, respectively, using the six-hourly 3D wind fields from the ECMWF operational analysis data; (ii) the second concerns air

271

272

273

274

275

276

277

279

280

281

282

283 284

285

286

287

288

289

290

291

292

293

294

295

296

297

298

299 300

301

302

303

304

305

306

307

308

309

310

311

312

313

314

315

316

317 318

319

320

321

322

323

parcel trajectories based on the ERA5 reanalysis wind fields for the 100 most extreme daily precipitation events in each of the two boxes, starting from the grid points in the Greece and Lybia boxes as for the first set of trajectories trajectories. These 100 extreme events were defined as the days with the highest number of grid points within the Libya or Greece region experiencing daily surface precipitation exceeding the 90th percentile for autumn in the years 1990 - 2023. Storm Daniel is among the 100 most extreme daily precipitation events for both regions. We interpolated specific humidity, relative humidity, and the boundary layer height pressure along all trajectories.

We identified moisture sources in Daniel and in the 100 most extreme daily precipitation events After calculating all the air parcel trajectories, we identified Daniel's moisture sources and those of with the 100 most extreme daily precipitation events using the moisture source diagnostic from Sodemann et al. (2008). ——This method involves the tracking of The changes in specific humidity along the trajectory are tracked for all trajectories that precipitate upon arrival, which are defined as air parcels showing a decrease in specific humidity during the last time step before arrival and a relative humidity larger than 90% upon arrival (following Sodemann et al., 2008). i.e., showing a decrease in specific humidity during the last step before arrival. If the specific humidity increases or decreases, a moisture uptake or loss, respectively, is recorded. All subsequent moisture uptakes or losses weight a moisture uptake. Along each trajectory, an increase in specific humidity is interpreted as a moisture uptake, and a decrease in specific humidity is interpreted as a moisture loss. Each moisture loss reduces all previous moisture uptakes, weighted by their uptake amount. For a detailed description of the moisture source diagnostic, see Sodemann et al. (2008). -The identified moisture uptakes along each trajectory were weighted by the decrease in specific humidity during the last step before arrival, and relative moisture uptakes over all trajectories were calculated for each six-hourly time step. Relative moisture uptakes are then gridded to a 1° global latitude/longitude grid and averaged for each day. The relative moisture uptakes are given in 10⁻⁵ % km⁻², representing each grid cell's relative contribution per km² to the precipitation in the target region. Finally, for the 100 most extreme events, the daily relative moisture sources are averaged over the 100 most extreme events are and used as a climatological reference for Daniel.

2.2.3 Attribution to climate change

We used the methodology developed in the rapid attribution framework "ClimaMmeter" (see Faranda et al. (2024,) for more details). ClimaMeter offers a dynamic approach to contextualizing and analyzing weather extremes within a climate context. This framework provides both easily understandable, immediate contextualization of extreme weather events and more in-depth technical analysis shortly after the events. In particular, we analyze analyze here how Mediterranean depressions landfalling in Greece and Libya have changed in the present (2001–2022; factual period) compared to what they would have looked like if they had occurred in the past (1979–2000; counterfactual period). To do so, we compute analogues of MSLP anomalies of Daniel from the MSWX database (Beck et al., 2022) and search for significant differences between present and past analogues in terms of pressure, near-surface temperature (t2m), precipitation (tp), and wind speed (wspd). To account for the seasonal cycle in surface pressure and temperature data, we remove the average pressure and temperature values for the corresponding calendar days at each grid point and each day. This removes the effect of varying surface elevation in space for surface pressure. Total precipitation and windspeed data are not preprocessed. If the duration of the event is longer than one day, we performed a moving average throughoutover the duration of the event on all variablesdatasets. We examined all daily surface pressure data for each period. We selected and selected the best 15 analogues, i.e., the data minimizing the Euclidean distance to the event itself. The number of 15 corresponding tos approximately to-the smallest 1% Euclidean distances in each subset of our data. We tested the extraction of 10 to 20 analogues, without finding qualitatively significant differences in our results. As customary in attribution studies, the event itself is excluded for the present period. Following Faranda et al. (2022), we defined quantities supporting our interpretation of analogue-based assignments. We can then compare these quantities between the counterfactual and factual periods. The quantities are:

326

327

- Analogue Quality (Q): Q is the average Euclidean distance of a given day from its 29 closest analogues. If the value of Q for the extreme event belongs to the same distribution as its analogues, then the event is not unprecedented, and attribution can be performed. If the Q value exceeds greater than its analogues, the event is unprecedented and, therefore, not attributable.

328 329 330

331

332

333

334

- Predictability Index (D): Using dynamical systems theory, we can compute the local dimension D of each SLP map (Faranda et al., 2017). The local dimension is a proxy for the number of active degrees of freedom of the field, meaning that the higher the D, the less predictable the temporal evolution of the SLP maps will be (Faranda et al., 2017). If the dimension D of the event analyzedanalysed is higher or lower than its analogues, then the extreme will be less or more predictable than the closest dynamical situations identified in the data.

335 336 337

338

339

- Persistence Index (Θ) : Another quantity derived from dynamical systems theory is the persistence Θ of a given configuration (Faranda et al., 2017). Persistence estimates the number of days for which we will likely observe a situationmap that is analoguouse to an analogue of the one under consideration. As with O and D, we compute the two values of persistence for the extreme event in the factual and counterfactual world and the corresponding distributions of persistence for the analogues.

340 341

343

344

345

346

347

348

349

350

351

352

353

Finally, to account for the possible influence of low-frequency modes of natural variability in explaining the differences between the two periods, we also considered the potential possible roles of the El Niño-Southern Oscillation (ENSO), the Atlantic Multidecadal Oscillation (AMO), and the Pacific Decadal Oscillation (PDO). We performed this analysis using monthly indices produced by NOAA/ERSSTv5. Data for ENSO and AMO were retrieved from the Royal Netherlands Meteorological Institute (KNMI) Climate Explorer. At the same time, the PDO time series was downloaded from the NOAA National Centers for Environmental Information (NCEI). The significance of the changes between the distributions of variables during the past and present periods was evaluated using a two-tailed Cramér-von Mises test at the 0.05 significance level. If the p-value is smaller than 0.05, the null hypothesis that both samples are from the same distribution is rejected, nNamely, we interpret the distributions as being significantly different. We use this test to determine the role of natural variability.

354

355 356

358

359

360

361

362

363

364

365

366

367

368

369

3. Atmospheric

processes

leading

to

impacts

3.1 Cyclogenesis stage and impacts in Greece

Before Daniel formed, an omega-blocking pattern and an anticyclonic Rossby wave-breaking occurred over Europe (Couto et al., 2024). Wave breaking resulted in the intrusion of an upper-level PV streamer into the central Mediterranean basin, triggering cyclogenesis in the Ionian Sea on 4 September 2023, which eventually led to the formation of Daniel within 24 hours (northernmost, first track point in Fig. 1a). Figure 2a shows that the cyclone on 5 September 2023 was located between Italy and Greece, developing as a moderate low-pressure system with a minimum MSLP value of about 1004 hPa. The PV streamer in the upper troposphere wrapped cyclonically around the cyclone centre (green contour in Fig. 2a), pointing out an ongoing baroclinicity, forcing the cyclone's development. Accordingly, a high wind speed pattern followsaligned with the PV streamer's orientation with larger values over the Balkansbalkans and at the northwest side of the cyclone (wind barbs in Fig. 2a). This configuration summarises a typical dynamical structure of Mediterranean cyclones at a stage preceding maturity, i.e., the time of maximum intensity (Flaounas et al., 2015).

370 371 372

373

374

375

376

377

378

Accumulated precipitation also follows the typical structure of Mediterranean cyclones, with higher amounts on the northeast side of the cyclone centre (Flaounas et al., 2018). Figure 2a shows that at the cyclone's initial stages, the highest precipitation accumulation was observed in central Greece (Dimitriou et al., 2024). The NOAAN surface stations recorded more than 750 mm of daily rainfall and up to 1,235 mm within four days in eastern parts of the Thessaly region (flooded areas are shown in cyan colours in Fig. 1b). NotablyIt is noteworthy that these peak values are underestimated by about 450% in the ECMWF analysis (max IFS 24-h# accumulated rainfall equal to 434 mm on 6

379 September 2023 00 UTCzpurple colours in Fig. 2a).

To quantify the contribution of local and remote areas to such an intense precipitation event in Greece, Fig. 3a identifies, the areas where moisture uptake has been significant for the air parcels that reached the flooded area of Thessaly (blue square in Fig. 3a), the areas where moisture uptake has been significant. Taking into consideration the largest moisture uptakes that contribute by at least 50% to the catastrophic precipitation in Greece (dashed b-second inner black contour in Fig. 3a that primarily mostly separates the green from the redoutlines green to red colours), major sources were found in the Aegean and the Black Seas. This tilted southwest-to-northeast orientation of essential water sources follows the pathway of strong winds blowing over the Balkans and the eastern Mediterranean (wind barbs in Fig. 2a), having a similar orientation concomitant to with the upperlevel PV streamer. The intense sea surface fluxes induced by easterly winds are a precursor feature in common with other cyclones developing in the same area (e.g., Miglietta et al., 2021). Further, moisture (light blue colours in Fig. 3a) mainly originated from central to eastern Europe and the North Atlantic Ocean. These source regions are in general agreement with a recent study (Argüeso et al., 2024), which investigated moisture sources of rainfall over Greece from 3 to 9 Sep 2023 using a Eulerian moisture source diagnostic. Our moisture source analysis shows larger contributions from land (54.7%) than in Argüeso et al. (2024) (27%). The Lagrangian method used in our study shows relatively large moisture contributions from north of the Black Sea because most of the air parcels arriving on 5 Sep 2023 descended and took up moisture in this region before moving southwestward along the western flank of the PV streamer. The differences in the land fraction between the two methods might originate from different periods used for the moisture source calculations, different handling of moisture uptakes above the boundary layer, a lower explained fraction of the total moisture sources (84%) with the Eulerian compared to the Lagrangian diagnostic (explained fraction of 90%), and general differences in Eulerian versus Lagrangian approaches. An ongoing comparison study of moisture source diagnostics is investigating differences in these methods in detail and will shed more light on disagreements between various moisture source diagnostics.

Overall, the moisture sources. This agrees well with the climatology of moisture sources of the Mediterranean cyclones that produce the most heavy precipitation events (Flaounas et al., 2019). The moisture sources shown in Fig. 3a largely overlap with the climatological moisture sources of extreme precipitation in the same area. However, for Daniel, they are mostly concentrated over the Aegean Sea and areas to the northeast. In contrast, the whereas the typical moisture sources for extreme precipitation in Thessaly extend further over the central Mediterranean (Fig. 3b). The moisture water sources shown in Fig. 3a come partly in contrast to the climatological moisture sources of extreme precipitation in the same area. Indeed, Fig. 3b shows that the water sources that typically contribute to extreme precipitation events in the region of Thessaly are mainly located in the Aegean Sea, extending westwards over the Mediterranean Sea in areas that somewhat overlap with the primary moisture—sources—for—Daniel—precipitation—event—in—Greece—(Fig. 3a).

The hydrological impacts of Storm Daniel were profound and unprecedented. Figure 4 compares the peak mean daily river discharge during Daniel with the historical records over three decades, integrating the cumulative hydrological impacts over the entire event. Figure 4a shows the spatial distribution of the maximum simulated peak discharge from January 1993 to August 2023 (i.e., before Daniel), demonstrating typical peak discharge patterns in the Eastern Mediterranean. On the other hand, Fig. 4b compares the event-wide mean daily peak discharge during September 2023, when Daniel occurred, against the historical peak discharges of the last 30 years in Fig. 4a. Results reveal an unprecedented magnitude of Daniel's impacts, with several areas experiencing discharges that exceeded the historical maximums by 300 to 500%. The darkest shades in Fig. 4b indicateindicates ignify the most heavily affected regions, where the river discharge during Daniel exceeded previous records by at least a factor of five, highlighting that Daniel was an unprecedented event of increased river discharge levels (further discussed in section 5). At this cyclone stage, 17 human casualties were registered in Thessaly, along with a profound hydrological aftermath. The extreme rainfall from 3 to 8 September 2023 led to widespread flooding across 1,150 km² in the Thessalian plain, 70% of which constituted agricultural land. The inundation severely affected the

435

436 437

438 439

440

441

442

443

444

445

446

447

448

449

450

451

452

453

454

455 456

457

458

459

460

461

462

463

464

465

466

467

468 469

470

471

472

473

474

475

476

477

478

479

480

481

482

483

484

485

486

487

488

cotton crops, with floodwaters covering more than 282 km², roughly 30% of the region's total cotton fields. Over 35,000 farm animals were also affected (He et al., 2023).

3.2 Mature stage and impacts in Libya

Severe weather events gradually faded in Greece during the night of 6 September 2023 while the surface cyclone moved southwards in phase with the upper-tropospheric low. In the following three days, Daniel lingered over the central Mediterranean Sea (circular part of the track in Fig. 1a), with minimum pressure remaining almost constant, close to 1004 hPa (Fig 1a). During this period, the sea surface temperature (SST) in the central Mediterranean has been anomalously high by roughly 2 K respect to the average September SST of the period 1982-2011 (Fig. 5a). Figure 5a, b shows the SST anomaly in the area affected by Storm Daniel on 3 and 9 September, respectively. Before the passage of Storm Daniel, positive SST anomalies dominated the study area, with values exceeding 1°C between the Libyan coast and Greece, and lower anomalies (0 to 0.5°C) observed east of Sicily. Following the storm's passage, a significant drop in SST resulted in an extensive area of negative anomalies greater than 1°C between Libya and Greece. A colder SST core with a decrease of less than 1.5°C was observed east of Sicily, while the northern Aegean Sea experienced an even more pronounced decline. Such SST cooling after the passage of medicanes has been previously diagnosed using explicitly resolved air-sea interactions in coupled atmosphere-ocean models (Ricchi et al., 2017; Bouin and Lebeaupin Brossier, 2020; Varlas et al., 2020) and SST observations (Avolio et al., 2024). Nevertheless, the feedback mechanism between cyclones intensity and SST cooling is expected to be less important than the one typically observed in tropical cyclones.

The role of anomalously high SSTs in intensifying cyclones has been previously shown in several studies based on numerical sensitivity experiments (Miglietta et al., 2011; Romaniello et al., 2015; Messmer et al., 2017; Pytharoulis, 2018, <u>Argüeso et al. 2024; Sanchez et al. 2024</u>). In the case of Daniel, deep moist convection was favoured, as suggested by the great extent of the areas covered by cold cloud-tops and intense lightning activity close to the cyclone centre (not shown). Afterward, on <u>8</u> September—8, the cyclone started showing tropical-like features, like deep warm core, spiral cloud bands, and a maximum wind speed in the low levels a few tens of km <u>far</u> from the centre. Thus, the cyclone satisfies the phenomenological definition of a medicane recently proposed (Miglietta et al., <u>submitted2025</u>). Deep convection contributed to the rapid deepening of the cyclone, <u>which reacheding</u> a minimum MSLP of 997 hPa on <u>109</u> September 2023, <u>18 UTCz</u>. <u>a</u>After <u>makingthat</u>, <u>Daniel made</u> landfall at the northeastern coasts of Libya <u>during the early morning around on around 101 night hours of 9 September 2023, 06000 UTC (Fig. 1)</u>. <u>It is worth mentioning to be mentioned that</u>

A comparison of Figs. 2a and 2b shows that, at the time of maturity, the area covered by at least 2 PVUs at 300 hPa is significantly smaller than during cyclogenesis. Nevertheless, Fig. 2b shows that the 2-PVU patch is collocated with the cyclone center, advected from the west. Hewson et al. (2024) proposed that this collocation is responsible for the cyclone's intensification just before making landfall. In fact, the synergistic intensification of a Mediterranean cyclone due to the synergy of both upper-level baroclinic forcing and deep convection is a common characteristic of intense Mediterranean cyclones, including medicanes (Flaounas et al., 2021). A previous case of a medicane intensifying due to the collocation of a PV streamer with the cyclone center was documented by Chaboureau et al. (2012). This phenomenon reflects, on the one hand, the anomalous nature of this medicane (as medicanes generally intensify over the sea and weaken inland)-and, on the other hand, the critical role of upper-level features in the evolution of Mediterranean cyclones. Comparison of Figs. 2a and 2b shows that at the time of maturity, the re is a smaller-extent of the area extent which is covered by at least 2-PVUsupper-level PV streamer at 300 hPa was weaker is rather smaller than during cyclogenesis. Nevertheless, At the same time, Daniel has developed a significantly stronger MSLP gradient, leading to wind speeds that reached up to 40 kts (about 20 m s⁻¹). Nevertheless, Fig. 2b shows that the 2-PVU patch area is collocated with the cyclone centre, being advected by the west. Hewson et al. (2024) While weaker than earlier, the wrap-up of the upper-level PV streamer around the cyclone centre was proposed this collocation to be responsible for theits intensification of the cyclone just before the cyclone made landfall (Hewson et al., 2024). The synergistic intensification of a Mediterranean cyclone due to both upper-level baroclinic forcing and deep convection has been

490

491

492

493

494

496

497

498

499

500

501

502

503

504

505

506

507

508

509

510

511

512

513

515

516

517

518

519

520

521

522

523

524

525

526

527

528

529

530

531

532

533

534

535 536

537

538

539

540 541

542

543

shown to be rather common for medicane systems and other intense Mediterranean cyclones (Flaounas et al., 2021), while a previous case of a medicane being intensified due to the collocation of a PV streamer with the cyclonce centre (Chaboureau et al., 2012). This reflects, on the one hand, the anomalous characteristics of this medicane (medicanes generally intensify over the sea and weaken inland), on the other hand, the critical role of upper level features for the evolution of Mediterranean cyclones.

At the same time, Daniel has developed a significantly stronger MSLP gradient, leading to wind speeds that reach up to 40 knotskts (about 20 m s-1). The intense winds associated with the storm generated a severely disturbed sea in the Central Mediterranean basin, with south-westerwardly propagating waves extending from the Aegean Sea to Libya following the strong winds pathway (Fig. 2b). Indeed, the analysis of the wave data from the Mediterranean Sea Waves Analysis and Forecast evinces waves with significant height of about 5 m in the Gulf of Sirte and the northern Aegean Sea (Fig. 6a). Such values exceed the 99th percentile in the Mediterranean Sea wave reanalysis. A peculiar aspect of Daniel is that strong winds blew in the Central Mediterranean Sea for many days. As a result, Daniel preserved a severe sea state over northern Greece, in the Central Mediterranean basin, and along the Libyan coast. To evaluate the cumulative impact of the event, we computed the total storm wave energy (TSWE; Arena et al., 2015) by integrating the wave power contribution of each sea state over the storm duration (Fig. 6b). TSWE reaches peak values of about 3000 kWh /m-1 in the Gulf of Sirte, which is above the 99th percentile of the total storm wave energy obtained from the Mediterranean Sea wave reanalysis. Such an energetic sea condition and the storm surge affected much of Libya's eastern coastal zones, causing coastal flooding, erosion, and infrastructure damage (World Bank, 2023). However, due to a lack of detailed information about coastal damages, it is impossible to evaluate the relative socioeconomic impact of each single threat (storm surge, waves, river flood) driven by

In terms of precipitation, Storm Daniel also presented exceptional features. During the cyclone's mature stage, Bayda experienced about 414.1 mm of rainfall within less than 24 hours, equaling 80% of the city's mean annual accumulated precipitation and a new daily precipitation record (Weather World Meteorological Organisation, 2023). It is worth mentioning that simulated 24-hr total accumulated precipitation on 11 September 2025 in Libya, up to 382 mm, was not located within the Derna catchment, as it has been discussed in Hewson et al. (2024), which was the most impacted area. Figure 3c shows sSignificant moisture sources (red colours in Fig. 3c) to encompass the cyclone centre with more than 50% of the moisture originating from the Mediterranean Sea. This suggests that the cyclone-induced circulation played an essential role in moistening the atmosphere within the proximity of the cyclone. Nevertheless, the largest moisture sources that contribute together -byto at least 5075% ofto the total precipitation-event in Libya (black dashed contour encompassing green to red colours in Fig. 3c) still retain a southwest-to-northeast orientation as in Fig. 3a (i.e., during the precipitation event in Greece). Comparing the moisture sources among the two precipitation events in Greece and Libya, it seems that the cyclone tends to attract more moisture from its surrounding area in the latter case in the latter case, the cyclone tends to attract more moisture from its surrounding area. -In contrast, in both cases, northern moisture sources tend to align with the large-scale circulation responsible for downstream cyclogenesis in the Mediterranean. This southwest-northeast orientation of moisture sources contrasts with the climatological sources in Figs. 3b and 3d, that mainly highlighting the importance of local sources, especially from the Mediterranean Sea westwards of the two study regions.

Figure 4 highlights the exceptional river discharges in the region, as in the case of Greece. However, the absence of similarly strong discharge signals in several severely impacted regions, such as the wider Pelion area in Greece and Derna (Libya), is notable and can be attributed to several factors. First, the GloFAS model has limitations in spatial resolution and calibration. The model operates at a resolution of approximately 5 km (0.05°), which, while adequate for global-scale flood awareness, is insufficient for resolving localized hydrological dynamics. For instance, the catchments east of Volos, including the wider Pelion area, are approximately 30 km2, while the Derna basin spans around 575 km2. In both cases, localized rainfall-runoff dynamics are critical in shaping discharge patterns,

particularly during extreme events. Due to insufficient in-situ discharge data, the absence of Greece and Libya in the GloFAS calibration dataset further exacerbates these limitations since the model relies on generalized parameter regionalization rather than site-specific calibration, introducing significant uncertainties into discharge predictions. Furthermore, inaccuracies in the rainfall inputs depicted in Figure 2 propagate into the discharge simulations shown in Figure 4. For instance, within the Peneus catchment, the maximum recorded 24-hour accumulated precipitation was 274 mm at Zappeio and 226 mm at Neraida stations, as Dimitriou et al. (2024) reported, while accumulations of up to 750 mm were recorded outside the catchment, specifically over the Pelion area, east of Volos. In the Wadi Derna catchment, extreme rainfall exceeded 400 mm day-1, with torrential rainfall ranging between 150 and 240 mm across several locations and Al-Bayda recording a maximum of 414.1 mm (WMO, 2023). These rainfall extremes were underrepresented in the GloFAS rainfall inputs, propagating into the discharge simulations and contributing to the muted signals observed in Figure 4(b).

Eventually, after landfall, Daniel dissipated fast over the Sahara Desert when it reached Egypt on 11 September 2023.

Daniel resulted in severe flash floods in northern Libya, with river discharges exceeding by 500% the peak values of the last three decades in the region (Fig. 4b). As a result, northeastern Libya's population of 884,000 people has been affected directly in five provinces by the collapse of two dams. About 30% of the city of Derna was flooded, and almost 900 buildings were destroyed, including damages to roads and other infrastructure in the area (OCHA 2023, UNICEF 2023). According to the DTM update (IOM 2023), over 5,000 people were presumed dead, 3,922 deaths were registered in hospitals, 10,000 people were declared missing by the Libyan government and Red Crescent Society while at least 30,000 people were recognized as internally displaced (UNICEF 2023, IOM 2023) in the Derna area. Extensive damage was shown to critical infrastructure such as hospitals and drinking water supply systems. Many roads were rendered impassable, making it difficult for humanitarian aid and supplies to get through. At least \$10 million budget was allocated from the UN Central Emergency Response Fund to scale up intervention in response to the Libya disaster, and almost 72 million were requested to cope with the most urgent needs of around 250,000 people (OCHA 2023) just for the first three months after the flooding.

4. Weather forecasting of Daniel and implications forto impacts

Daniel's impacts took place in two distinct periods: during cyclogenesis and at maturity. In the former stage, most precipitation was produced in areas <u>far from remote to</u> the cyclone centre, drawing moisture from the <u>broader</u> surrounding areas. At the later stage, the cyclone impacts were relevant around landfall, and precipitation and sea level rise were important close to the cyclone centre. Therefore, the two distinct stages of Daniel that provoked substantial impacts in Greece and Libya were linked to cyclone stages of different dynamics, which also have <u>otherdifferent</u> implications in Daniel's numerical prediction. In the case of Greece, i.e., at the initial stage of Daniel, it is the timely prediction of cyclogenesis that would <u>have</u> primarily provided useful information to civil protection, whereas, in the case of Libya, it <u>would have beenis</u> the accurate prediction of the cyclone track, intensification, and its landfall location. This section focuses on the predictability of the environmental hazards linked to Daniel's socio-economic impacts, i.e., precipitation amounts, sea state, and cyclone track.

4.1 Forecasting cyclogenesis stage

Concerning the cyclogenesis stage, a forecast model has to predict the formation of the cyclone <u>toin</u> order to provide valuable information regarding its impact. This suggests that numerical weather prediction <u>models</u> should accurately reproduce the large-scale atmospheric circulation, the Rossby wave breaking, and the consequent intrusion of the PV streamer within the Mediterranean, as shown in Fig. 2a by the green contour. <u>Such a large-scale circulation pattern is absent from forecasts initialised one week ahead (Fig. 7a)</u>. At a lead time of <u>12096</u> hours, the PV streamer intrusion is <u>present but with Fig. 7a shows</u> high uncertainty among the EPS members on <u>itsthe</u> location (Fig. 7c) of the PV streamer intrusion. Indeed, the <u>average PV distribution</u> of all EPS members of <u>ECMWF</u> at

 300 hPa (outlined by <u>coloured crosses</u><u>blue contours</u> in Fig. 7) depicts a much larger area of <u>possible</u> high PV values than the one in Fig. 2a. This is due to the limited agreement on the occurrence -or colocation- of the intrusion of the PV streamer among the EPS members, of the order of 25 to 50%, as suggested by the blue crosses in Fig. 7ca.

Following the uncertainty in the PV streamer occurrence, the cyclone is also absent from the MSLP ensemble average values—one week ahead (black contour in Fig. 7a) and the MSLP spread seems rather consistent within the shown domain (about 1 to 3hPa) is also high around in Fig. 7a with no clear local minimum in the average values at a lead time of 12096 hours (shading in black contour in Fig. 7ac). At subsequent lead times, higherthe spread of MSLP tends to concentrate close to the cyclone centredecreases (Figsd 7c and 7ee.g., Fig.s 7c and 7e) until it becomes negligible 24 hours before cyclogenesis (Fig. 7g). At such a shortsuch short lead times, the cyclone formation was forecasted with confidence to occur in the Ionian Sea, to the southwest of Greece (black contours in Fig. 7g). Confident forecasts of cyclogenesis should go hand in hand with higher agreement among the EPS members on the location of the PV streamer. Indeed, 24 hours before cyclogenesis, more than 95% of EPS members agreed on the area of PV streamer intrusion. AccordinglyIn contrast, average values (blue contour in Fig. 7g) better match the ones in the ECMWF analysis (green contour in Fig. 2a).

The similar behaviour in the spread of MSLP and PV streamer relies on the direct relationship between the Rossby wave breaking over the Atlantic Ocean and the accurate prediction of Mediterranean cyclogenesis. In the case of Daniel, This has been highlighted by Chaboureau et al. (2012) and, more recently, by Portmann et al. (2020) and Sherrmann et al. (2023). It has also been discussed in a review paper by Flaounas et al. (2022).

To get deeper insights into the representation of cyclogenesis among the EPS members, Fig. 8 shows the level of agreement on the cyclone objects (as presented in section 2.2.1). At- a lead times of 168 hours, forecast cyclogenesis forecast was rather poor (Fig. 8a), but aAt a lead times of 12096 hours (Fig. 8ca), cyclone centres are present (red dots in Fig. 8), scattered inacross the central Mediterranean but still close to the actual location where the cyclone was initially formed while two members of the EPS do not even predict cyclogenesis. Higher overlapping of cyclone objects among the EPS members (green shading in Fig. 8) is indeed within the limits of the observed cyclone object as in the ECMWF analysis (black contour in Fig. 8ca). In fact, about 30% of the different EPS members produce overlapping cyclone objects. At a forecast lead times of three days, the overlapping of cyclone objects increases clearlyabruptly (comparing green shaded areas between Figs 8ca and 8ce), suggesting a much higher agreement among the EPS members on the cyclone occurrence within the correct location. The high agreement is retained also for shorter lead times of two and one days (Fig.s 8c and 8g).

The similar behaviour in the cyclone and PV streamer predictability predictability of the cyclone and PV streamer—relies on the direct relationship between the Rossby wave breaking over the Atlantic Ocean and the accurate prediction of Mediterranean cyclogenesis. This has been highlighted by Chaboureau et al. (2012) and Pantillon et al. (2013) for thea case of the extratropical transition of a hurricane upstream of a medicane—and, more recently, by Portmann et al. (2020) for another case and has been demonstrated by Sherrmann et al. (2023) in a semi-idealized frameworkfor other cases. In the case of Daniel, Hewson et al. (2024) similarly suggested the role of the extratropical transition of Hurricane Franklin as responsible for theofin the high uncertainty one week ahead. Only in forecasts initialized after the extratropical transition has occurred is the PV streamer the PV streamer is predicted to intrude on the Mediterranean, thus explaining the contrast between 5 and –7 days lead times. A similar "jump" in the predictability of cyclone occurrence has been shown for several medicane cases by Di Muzio et al. (2019). Most probably, this "jump" is due to the dependence of Mediterranean cyclogenesis on the preceding Rossby wave breaking and, consequently, on the credible inclusion of this event within the forecast initial conditions.

4.2 Forecasting cyclone location and intensity at the mature stage

Figure 1a shows that on 10 September, Daniel was at its mature stage and—made landfall on the coasts of Libya. For all different forecast lead times of this event—shown in Fig. 7, the spread of MSLP consistently retains high values close to the landfalling area (right column of panels in Fig. 7). This is directly relevant to the high MSLP gradients close to the cyclone centre (Fig. 2b) where negligible displacement of cyclone centres may result in a relatively large standard deviation of MSLP in the EPS. Indeed, Figs. 8b and 8d point to the high certainty of the cyclone occurrence in the EPS, where most members produce consistent and overlapping cyclone objects (depicted by dark green shading—in Figs. 8b and 8d). Such performance comes in contrast to forecasting the stage of cyclogenesis, where MSLP spread does not have a clear pattern (in-the left panels of Fig. 7,—(green and yellow areas), and cyclone objects present limited overlapping for the same lead times (e.g., comparing Figs 8 ca and 8db). The limited agreement among the EPS members on the PV streamer intrusion leads to considerable differences among the EPS members on the location or even the occurrence of cyclogenesis Daniel. In contrast, the predictability of landfall in Libya seems more consistent among the EPS members of ECMWF.

Considering <u>a</u> forecast lead times of <u>12072</u> to <u>96</u> hours (i.e., initialization on <u>66 or 7</u> September), the cyclone has already formed and was located over the central Mediterranean (<u>just before the</u> spiral part of the track). It is in the middle of its lifespan and increasing in intensity (MSLP depicted by dot sizes in Fig. 1a). Therefore, the cyclone has <u>already beenbeen already</u> inscribed in the model's initial conditions. Still, from the perspective of impacts, the location of landfall and the cyclone's intensity are crucial. Figure <u>910</u>a shows that even for <u>an</u> early lead times of <u>five5six</u> days (initial conditions of <u>54</u> September 2023, 0000 UTC), the cyclone tracks from all EPS members make landfall on the Libyan coasts. The spread of the tracks is wide enough to include the actual cyclone track (in blue colour in Fig. <u>910</u>a); therefore, the forecast may lead to a reliable and timely warning of potential impacts.

Nevertheless, Fig. 910b shows that almost all the EPS members underestimated the cyclone's intensity by forecasting too high MSLP values on 10 September at the time of landfall. The intensity of the cyclone is dependent on the baroclinic and diabatic forcing of its development (Flaounas et al., 2021). Therefore, the performance of all EPS members depends on the accurate representation of the parametrized processes, mainly convection close to the cyclone centre and surface fluxes, and the morphology of the PV streamer intrusion. For the present case, Hewson et al. (2024) noted that, while in the development stage, the latent heat released from convection, favoured by the high SST and intense sea surface fluxes, balanced out the tendency for frictional decay, in the last stage a marked upper-level low moving from the west (marked by high PV values in Fig. 7h)- was responsible for a further deepening. Upper tropospheric forcing is crucial in accurately predicting cyclone intensity in this context In this context, upper tropospheric forcing is crucial plays appears to play a crucial role in accurately predicting cyclone intensity. While Fig. 7b—unlike Fig. 7a—shows that somemore EPS members align with the location of the "this important upper tropospheric forcing feature" (blue crosses), an average of 2 PVU and an agreement above 50 % among the EPS members near the cyclone center is only evident at a lead time of approximately three days (Fig. 7f, depicted by green crosses).

5. Daniel's impacts in a climatological context

5.1 Forecasting climate extremes

The previous sections focused on the capacity of the EPS to forecast Daniel cyclogenesis as the primary driver of impacts. In this section, we extend this analysis by focusing on the predictability of hazardsimpacts in a climatological context, namely extreme precipitation and consequent floods. We used the ERA5 reanalysis to diagnose extremes since this product offers a reliable and consistent representation of present-day climate (Hersbach et al., 2020). In this respect, the left column of Fig. 109 shows the area affected by extreme daily precipitation on 5 September 5 (in red contour, explained in Section 2.2.1). In addition, Fig. 109 shows the percentage of the EPS members that forecast daily precipitation exceeding the climatological threshold for extremes, defined by the (99th percentile of daily precipitation in ERA5) of extremes (in blue shading). At a lead time of 1209

hours (Fig. 10c9a), less than half of the ensemble members predicted the climatological extreme precipitation amounts within the area delimited by the climatological values of ERA5 (red contours). Nevertheless, the area formed by the blue shading in Fig. 10c9b is consistent with the climatological extremes. It seems that Consequently, the members of the EPS that produce extreme precipitation could provide information at least fivefour days before issuing a warning on the potential occurrence of high-impact weather at least five days in advancebefore. Therefore, accurately forecasting the time and location of cyclone formation (as shown in Fig. 8) may play a secondary role in predicting its impacts in Greece. In this context, the reliable simulation of moisture inflow—which appears to be more closely linked to large-scale circulation, as previously discussed—by the EPS members could be more crucial for impact prediction.

Interestingly, the overlap of extreme precipitation objects among the EPS members might exceed 70% reach up to about 85% in the area of Thessaly in Greece for a lead time of even 12096 hours (Fig. 10c9a). This percentage is significantly higher thanexceeds by 52% the maximum percentage of overlap between the cyclone objects (Fig. 8ca). This suggests that the EPS members have been more consistent in the production of extreme precipitation even if cyclone centres presented a comparably greater spread. For subsequent lead times, the predictability of extreme precipitation strongly increases, showing a high probability for a lead time of even 72 hours. Indeed, almost all members predict extreme precipitation off the coast and in the northeastern part of Greece within the eventually flooded area of Thessaly.

WhenAt the time of the landfall of Daniel made landfall and produced impacts on the Libyan coasts, the EPS showed a higher predictability, with cyclone objects and associated extreme precipitation being predicted at least fivefour days in advance by several EPS members (Figs. 10d9b), albeit the location of both cyclone and precipitation objects are still displacedshifted to the southwest compared to the analysis (Figs. 8db and 10d9b). This comes in accordance with the southern displacement of several ensemble member tracks in Fig. 9a. The probability strongly increasesd at shorter lead times (Figs 10f and 10h9d, 9f and 9h). This shift is plausibly relevant to the change in Daniel's tracks in EPS members to the west side of the observed one (Fig. 10a), and it is mostlypretty corrected and all EPS members tend to converge to similar cyclone locations when reaching a lead time of one two day (Fig. 8h)s with a limited bias in the location of the cyclone centre towards the southwest.

The potential of extreme precipitation leading to substantial socio-economic impacts has also been transferred to hydrologic discharge forecasts. The hydrographs presented in Fig. 11 examine river discharge predictability as forecasted by the operational European Flood Awareness System (EFAS) during Daniel, For the Peneus Pineios-River outlet in Thessaly, the forecast initiated on 1 September underpredicted the peak discharge on 5 September. Nevertheless, extreme discharges were evident for several members five days in advance. The forecast accuracy improved getting closer to the event, with ensemble members (grey stripeslines) converging towards the peak discharge ("perfect forecast" - red line). This trend indicates an increasing reliability of the forecast as the lead time decreases, particularly within 48 hours of the event. Concerning the predictability of floods at the Wandi Derna River outlet (Fig. 11, right column), a similar pattern was observed as for the PeneusPineios River outlet. Initial forecasts are widespread among ensemble forecast members, reflecting high uncertainty. Nevertheless, as the lead time decreases, the ensemble forecast for 10 September aligns more closely with the actual discharge. The skill in discharge predictability for the Peneus River can be attributed, in part, to the large size of the basin (11.063 sq.-km2), which aligns relatively well with the spatial resolution of the EFAS model, enabling anmore accurate representation of distributed hydrological processes and moderating runoff variability.

The forecasts for the Wadi Derna River outlet (Fig. 11, right panels) exhibit significant variability and fail to converge during the earlier forecast initialization dates as well as at shorter lead times. This persistent lack of convergence can be attributed to distinct challenges of both temporal scales. For earlier forecast initialization dates, the primary source of variability lies in the westward displacement of extreme precipitation predicted by the EPS (Figs. 10b and 10d). For example, forecasts initialized on 9 September, during a critical period for implementing preventative measures, display a wide

 spread and a shortfall in the median forecast compared to the benchmark (red line). This variability persists even for forecasts initialized on 10 September. The failure to converge at shorter lead times is compounded by challenges inherent to the Wadi Derna catchment. The resolution of the precipitation forcings used in the forecasts combined with the relatively small size (575 km2) and flash-flood-prone nature of this basin amplify the uncertainties in predicting discharge, particularly in response to localized extreme rainfall.

Figure 4 provides critical context by comparing the peak mean daily river discharge during Storm Daniel with the historical baseline. The unprecedented magnitude of the event is evident in Fig. 4b, where discharges exceeded the historical reanalysis by at least fivefold in certain regions. However, the relatively weak signal for the Wadi Derna catchment underscores the limitations of the GloFAS and EFAS systems in accurately resolving runoff dynamics in smaller basins. This discrepancy is primarily attributed to insufficient model resolution, inaccuracies in rainfall inputs, and the lack of detailed hydrological calibration for these catchments. In contrast, the much stronger signal observed in the Peneus catchment aligns with larger basin sizes and better-resolved hydrological processes, where models more effectively captured the extreme nature of the event.

The ability of EFAS to predict extreme events, as shown in Fig. 11, highlights its value in forecasting severe hydrological impacts. However, discrepancies in simulated peak discharge remain apparent, such as the overestimation of runoff for the Peneus River outlet. EFAS simulated peak discharge at approximately 5000 m³ s-1, whereas observed values, based on station-level data and H-Q curve estimates, were less than 2000 m³ s-1 (Dimitriou et al, 2024). This overestimation reflects inherent limitations in the model's spatial resolution and hydrological representation. Furthermore, the absence of flood protection infrastructure, such as levees or dams that attenuate runoff and peak flows is not accounted for in the EFAS and GloFAS systems, contributing to these discrepancies. Additionally, the simplified representation of retention processes, including floodplain storage and wetland buffering, further amplifies discharge estimates in some regions. For smaller basins such as Wadi Derna, the rapid hydrological response to localized extreme rainfall presents additional challenges. The variability in rainfall distribution, coupled with the model's limited ability to capture localized hydrological dynamics, results in a weaker signal for the catchment, even during an event as extreme as Storm Daniel. These limitations emphasize the need for improved model resolution, enhanced precipitation forcings, and better calibration tailored to local catchment characteristics.

Nonetheless, the ability of EFAS to predict extreme discharges, particularly within short lead times, demonstrates the potential of operational forecast systems in capturing the extreme values of such events. Supported by EFAS and GloFAS, the Copernicus Emergency Management Service (CEMS) provides critical insights into the timing and magnitude of extreme hydrological events. These forecasts are vital for enhancing preparedness and response strategies in the face of escalating climate extremes, offering essential tools for civil protection efforts and mitigating the socio-economic impacts of such disasters.

Figure. 4 provides a crucial context by comparing the peak mean daily river discharge during Daniel with historical records over three decades. The unprecedented magnitude of the event, as shown in Fig. 4b, underscores Daniel's severity, which is especially evident in the darkest shaded regions where discharges were at least fivefold higher than in historical records. The ability of EFAS to predict such extreme events, as illustrated in Fig. 11, highlights its value in anticipating extreme events. Accurately predicting these unprecedented discharges, especially within a short lead time, suggests that operational forecast systems like EFAS can capture these events' extremities. The Copernicus Emergency Management Service (CESM), supported by EFAS and GloFAS, effectively predicts both the timing and magnitude of extreme hydrologic events, offering vital information that can enhance preparedness and response strategies in the face of escalating climate extremes. This capability is crucial for civil protection and mitigating such disasters' socio-economic impacts.

5.2 Attribution to climate change

820

821

822

823

824

825

826

827

828

829

830

831

832

833

834

835

836

837

838

839

840

841

842

843

844

845

846

847

848

849

850

851

852

853

854

855

856

857

858

859

860

861

862

863

864

865

866

867

868 869

870

871

872

We assess Daniel's attributionability to climate change using ClimaMeter's analogue-based approach (Faranda et al., 2024). By comparing surface pressure patterns in the periodsfrom 1979–2000 ("past") and 2001–present ("current"), we identify how similar Mediterranean depressions have evolved. We use MSWX data to Using MSWX data, we analyze changes in temperature, precipitation, and wind speed associated with these analogues, attributing observed shifts to anthropogenic climate change. We repeat the analysis twice, once for 5-6 September—5-6, when Daniel impacted Greece,;—and once for 10-11 September—10-11, when Daniel impacted Libya.

In this section, we discuss the attributability of Daniel and its hazards to climate change, using the approach used in ClimaMeter (see www.climameter.org and Faranda et al., 2024). The workflow used in ClimaMeter consists of looking for weather conditions similar to those that caused the extreme event of interest. The search of similar past events is based on defining analogues of the identified surface pressure patterns over the chosen spatio-temporal domain. We split the dataset 1979-Present in two parts of equal length and consider the first half of the satellite era as "past" and the second part as "present" separately. We use data from MSWX. We consider the first period as representative of a past world with a weaker anthropogenic influence on climate than the second period, which represents the present world affected by anthropogenic climate change. The analogues search is only performed on surface pressure data. Results reported for temperature, precipitation and wind-speed data are always associated with surface pressure analogues. About impacts in Greece, we search analogues for 5 September 2023 within the region defined within the domain shown in Fig. 12a and within the extended autumn season, from September to December (SOND). Results are reported in Fig. 12. Figure 12a-d shows that cyclone systems similar to Daniel's impactinglandfalling over Greece have about the same order of pressure minima in their centre as they didin the present asthan they had in the past-. Figure 12e-h shows that temperature during depressions hashave increased inon the Ionian Seasea byof about 2°C and decreased over Anatolia. Precipitation analysis (Fig. 12j-l) showsshow that similar events produce heavier precipitation over the Ionian Seasea and Albania but generally lower precipitation amounts over continental Greece and the Peloponnese (between 4 and 12 mm/day-1). The metrics Q, D, and Θ (Figs 12q-s) are computed to discuss changes in the possible dynamical properties of the eventToIn order to discuss changes in the possible dynamical properties of the event, the metrics Q, D, and Θ (Figs 12q-s) are computed. Q is defined as the mean Euclidean distance from the event to its best analogues, D is a metric of predictability and Θ study the persistence all the cyclones (see Faranda et al. (2022) for a detailed description of the metric. Figs 12q-s show no significant changes between the two periods (present and past climate). -We can, however, infer how close the event is to its analogues using the metric Q, which further highlights that the event has -similar analogues in past and present periods. Significance of the changes between the distributions of variables during the past and present periods is evaluated using a two-tailed Cramérvon Mises test at the 0.05 significance level. If the p-value is smaller than 0.05, the null hypothesis that both samples are from the same distribution is rejected, namely we interpret the distributions as being significantly different. We also find that similar events have become more frequent in December, while they previously occurred mainlychiefly in October, (Fig. 12t). Tolin order to evaluate the possible role of low-frequency modes of natural variability in explaining the differences between the composite maps of analogues in the two periods, e also include in our analysis monthly indices of the El Niño Southern Oscillation (ENSO), the Atlantic Multidecadal Oscillation (AMO), and the Pacific Decadal Oscillation (PDO). Www compare the distributions of the ENSO, AMO, and PDO values on the dates of the analogues in the past and present periods, and we test the statistical significance of the observed differences. For this date, our analysis suggests that natural climate variability, particularly the AMO and PDO, may have influenced the development of the MSLP pattern associated with the storm (Figs. 12u-w).

For storm Danielthis case, we find that the AMO and PDO sources of natural climate variability may have influenced the event (Figs 12u-w). This suggests that the changes we see in the event compared to the past may be due to a combination of human-driven climate change and natural variability. To clarify the trend in the frequency of these events, Fig. ure 12x considers in each period 30 analogues instead of 15, showing an increase in their number.

Regarding landfall in Libya, we searched for analogues We repeat the analysis for 10-11 September 2023 within the region depicted in Fig. 13a and search for analogues for the extended autumn season (SOND). Results are reported in Fig. 13. The MSLP changes (Fig. 13d) show no substantial differences in the areas that were significantly affected. The temperature T2M changes (Fig. 13h) reachshow up to $\pm 2^{\circ}$ C warmer temperatures on the east part of the domain. Precipitation changes (Fig. 13l) indicate that similar events produced higher precipitation amounts along the eastern Libyan coast (between 5 and 9 mm /day-1), which experienced intense rainfall from Daniel on 10 September 2023. The metrics Q, D, and Θ (Figs. 13q-s) show no significant differences between the two periods. While the 5 September analysis of Q identified suitable analogues, here, Q indicates that no good analogues are available, underscoring the exceptional nature of Daniel's pressure pattern when the storm impacted Libya.

We repeat the analysis for 10 September 2023 within the region depicted by Fig. 13a, and we searched for analogues for the extended autumn season (SOND). Results are reported in Fig. 13. The MSLP changes (Fig. 13d) show no substantial differences in the areas that have been strongly affected significantly. Precipitation changes (Fig. 13l) show that similar events produced larger amounts of precipitation in the eastern Libyan coast (between 5 and 9 mm/day), which was also severely affected by Daniel's severe precipitation on 10 September 2023. The metrics Q, D, and Θ (Figs 13q-s) show no significant changes between the two periods. While for the 5 of September the analysis of Q showed suitable analogues, here Q show that no good analogues are available, highlighting the exceptionality of the prerssure pattern of Daniel when the storm hit LibyaQ hereagain highlights that the event does not have suitable analogues in past and present periods. Events have become less frequent in September and November and slightly more common in December (Fig. 13t). As for 5 September-5, we find that AMO and PDO may have influenced the development of the MSLP pattern associated with the storm (Figs. 13u-w).

Finally, we find that sources of large-scale natural climate variability, namely the AMO and the PDO may have influenced the event (Figs 13u-w). Figure 13x showedshows changes in the frequency of these events when 30 analogues were searched for the entire period analyzedanalysed. As in the case of impacts in Greece, a significant increasing trend in frequency is found.

The analogues method helps us understanding extreme weather events like Daniel by comparing them to similar past events and seeing how they have changed over time. This allows us to assess whether climate change has influenced the storm's characteristics. While large-scale climate variability modes such as ENSO, AMO, and PDO can influence atmospheric conditions, our analysis does not establish a direct causal link between these modes and the development of Daniel; insteadrather, this assessment is exploratory, highlighting potential associations without making definitive attributions given the limitations of a 40-year dataset.

For 5 September, when Daniel impacted Greece, we found similar past Mediterranean storms, suggesting that this part of the storm's track was unusual but not unprecedented. Since we see no major changes in the MSLP pattern, the increase in precipitation over the region is most likely linked to higher sea surface temperatures (SSTs), which provideprovided more moisture to the atmosphere. This matches other studies that show showing that Greece experienced particularly strong moisture anomalies.

For 10-11 September, when Daniel reached Libya, our method found no suitablegood past matches, highlighting the exceptional nature of the storm's pressure pattern at this stage. However, like in Greece, we do not see substantial changes in MSLP, meaning that the increase in rainfall over Libya was also likely driven by warmer SSTs —and a warmer atmosphere, which can hold more water (Clausius—Clapeyron relationship) rather than a shift in atmospheric dynamics patterns. The MSWX dataset provides a reliable representation of large-scale atmospheric patterns but does not fully capture localized extreme precipitation intensities, which explains why our figures underestimate the observed rainfall totals, particularly in Libya; therefore, our analysis should be interpreted as reflecting broader climatological trends rather than exact station-level extremes. Importantly, while Daniel brought heavy rainfall, the disaster in Derna was mainly caused by the failure of poorly maintained dams (Shirzaei et al., 2025). DenteArmon et al. (2024) confirmeonfirms this, showing that while rainfall

was intense, it was not so extreme enough on its own to explain the scale of destruction—factors like unsafe building locations and poor emergency response played a major role.

These considerationsis analysis underscores a key point: while climate change can amplify precipitation by increasing SSTs, the most severe impacts often depend on societal factors such as infrastructure resilience and disaster preparedness.

Based on the analyses above, we conclude that Mediterranean depressions like Daniel hitting Greece and Libya show lower MSLP and higher precipitation in the present climate than in the past. We thus interpret Daniel as an event whose characteristics can be ascribed to human-driven climate change. Although not included in our analysis, we hypothesise that the changes we see in precipitation amounts compared to the past may be partially due to human-driven climate change, in keeping with the potential for heavier precipitation in a warmer climate.

6. Summary and conclusions

In the last decade, more than 410,000 deaths have been attributed to weather-related disasters, mostly in low-income countries where heatwaves and intense precipitation events are the leading causes of death. Aside from human casualties, 1.7 billion people have been affected in the 2010-2020 decade by these kinds of phenomena. The IFRC World Disasters Report (2020) concluded that the climate acts as a risk multiplier, especially in the case of low-income countries andor-even at a regional level thereininside countries. A glaring example of the impact of such disasters has been highlighted by the recent floods in the Mediterranean, especially in Greece and Libya, following the Mediterranean cyclone Daniel.

This study aimed to comprehensively <u>analyzeanalyse</u> medicane Daniel, which links atmospheric dynamics, predictability, and impacts. Beyond the description of the underlying physical processes, atmospheric dynamics are used here to understand the performance of numerical weather prediction <u>models</u>. Impacts, in terms of —floods and sea state (for Libya), have also been <u>analyzedanalysed concerningwith respect to numerical weather prediction models</u>. <u>Our analysis has been framed by the climatological context of All of our analysis has been framed by the climatological context of both cyclone-induced precipitation and relevant impacts that link with climate change attribution of both catastrophic events.</u>

From the perspective of atmospheric dynamics, the processes governing Daniel were similar to those identified for other intense Mediterranean cyclones: cyclogenesis was triggered by the intrusion of an upper-level PV streamer in the Ionian Sea, and thereafter, the cyclone developed into a deep storm, that propagated southwards and towards Libya while it was turning into a well defined mesoscale tropical-like cyclonic system. Regarding In terms of impacts, we identified two well-distinct stages: the first is relevant to cyclogenesis, where Daniel was newly formed and affected Greece with severe floods (on 5 September, 2023). In the second stage, Daniel reached maturity while making landfall in Libya, where it inflicted severe socio-economic impacts on 10 September 2023 due to floods (about 5 days after the floods in Greece). Daniel produced extreme precipitation in both stages In both stages, Daniel produced extreme precipitation amounts, driving a moisture flow towards the areas that experienced the floods. The moisture transport <u>followedwas</u>-aligned with <u>the large-scale atmospheric</u> circulationaligned with the PV streamer, particularly and, in particular, the large-scale atmospheric circulation with. Lwith large amounts of moisture that contributed to the catastrophic precipitation in the flooded areas were drawn locally from the Mediterranean Sea, which has been anomalously warm, from the continental regions ofareas of central and eastern

In Greece, the floods occurred <u>relatively remotelyin</u> a relatively remote areaan area that was rather remote from the cyclone centre. On the other hand, floods in Libya occurred close to the cyclone centre. Therefore, the implication of different cyclone dynamics is important in <u>predictingthe prediction of socio-economic impacts at both weather and climate scales. During its first stage <u>inover Greece</u>, the predictability of the cyclone formation was <u>relativelyrather</u> poor for lead times of more</u>

than four days. <u>ItIn fact, it</u> was a rather challenging issue for the ECMWF EPS to forecast precisely the intrusion of the PV streamer in the Mediterranean. This result aligns with previous studies that showed <u>relativelyrather</u> poor performance in predicting medicane occurrences for lead times of the order of four to five days (Di Muzio et al., 2019). <u>With higher confidence confcertaintyFor shorter lead times</u>, the ECMWF EPS could forecast cyclogenesis, and thus the flooding event, <u>for shorter lead times with higher certainty</u>.

During its second stage (impacts in Libya), the cyclone intensified quickly, transitioned into a medicane, and made landfall in Libya within a few days. The predictability of the medicane track -and therefore its landfall- showed higher certainty for lead times of four days. This suggests that numerical weather prediction <u>models areis</u> more prone to an erroneous predictability of the stage of cyclogenesis, i.e., after the cyclone formed, it is more likely for a forecast model <u>to correctly predict predict</u> correctly <u>its evolution in terms of location. in subsequent times correctly to correctly predict its location in subsequent times.</u>

Precipitation amounts were found to correspond to climate extremes in both_countries, Greece and Libya, where. In both cases, floods were responsible for_unprecedented river discharges that largely exceeded the climatological maxima of the last 20 years. The numerical weather prediction model couldwas able to forecast these climate extremes (even if thresholds were defined by reanalysis and not by the same forecast model). This suggests the exceptional potential for information to the public about the severity of imminent high-impact weather. Indeed, framing weather forecasts into a climatological context, e.g., providing a precipitation event's return period providing a return period of a precipitation event, would provide the means to the local population for an empirical assessment of the severity of an imminent high-impact weather event. In this context, we have analyzedanalysed Daniel concerningwith respect to climate change, and we have provided the grounds to interpret Daniel as an event whose characteristics can be ascribed to human-driven climate change. In these regards, we have performed an analysis based on analogues; indeed, several cyclones with similar characteristics and indeed several of them were found during winter. The anomalous occurrence of such a storm in September, a warmer month for SST, could be a reason for enhancing its destructiveness through enhanced precipitation.

In the scientific literature, weather events are typically analysed as case studies with specific objectives that rarely escape the narrow scope of a single scientific discipline. Here, we used Daniel, a high-impact weather event, as a centrepiece of different approaches toin order to better understandprovide a deeper understanding of socioeconomic impacts through the prism of both weather and climate scales. We find such an approach valuable for the bridging of different scientific communities and eventually important for communicating the communication of hazards to the local population. We envisage using the use of this interdisciplinary approach for other weather extremes and regions.

Acknowledgements

We gratefully acknowledge Ambrogio Volontè and an anonymous reviewer for accurately reviewing our paper. This article is based upon collaborative work of two COST Actions: from COST Action—CA19109 "MedCyclones" and CA22162 "FutureMed", supported by COST — European Cooperation in Science and Technology (http://www.cost.eu, last access: 1420 FebruaryJuly 20254) and from project "Earth Observations as a cornerstone to the understanding and prediction of tropical like cyclone risk in the Mediterranean (MEDICANES)", ESA Contract No. 4000144111/23/I-KE. Georgios Kyros from the National Observatory of Athens/meteo.gr is acknowledged for helping collect the Copernicus Sentinel-2 data in Figure 1. The Israel Science Foundation (grant \#978/23) funds, provides funding for AH's contribution. PP was funded by the EU's Horizon Europe program, OCEANIDS (G.A. No. 101112919). SD acknowledges the support from Next Generation EU, Mission 4, Component 1, CUP B53D23007490006, project "Exploring Atmospheric Rivers in the Mediterranean and their connection with extreme hydrometeorological events over Italy: observation, modelling and impacts (ARMEX)". We thank Franziska Aemisegger for providing the msd-cpp code for the calculation of the moisture sources.

1038 7. References

1039 Argüeso, D., Marcos, M. and Amores, A.: Storm Daniel fueled by anomalously high sea surface 1040 temperatures in the Mediterranean, npj Clim Atmos Sci 7, 307, https://doi.org/10.1038/s41612-1041 024-00872-2, 2024.

1042 1043

Avolio, E., Fanelli, C., Pisano, A. and Miglietta, M. M.: Unveiling the relationship between Mediterranean tropical-like cyclones and rising Sea Surface Temperature. Geophysical Research Letters 51, e2024GL109921, https://doi.org/10.1029/2024GL109921, 2024.

1045 1046

1044

1047 Beck, H. E., Van Dijk, A. I. J. M., Larraondo, P. R., McVicar, T. R., Pan, M., Dutra, E., and Miralles, 1048 D. G.: MSWX: Global 3-Hourly 0.1° Bias-Corrected Meteorological Data Including Near-Real-Time Updates and Forecast Ensembles, Bulletin of the American Meteorological Society, 103, E710–E732, 1049 1050 https://doi.org/10.1175/BAMS-D-21-0145.1, 2022.

1051 1052

1053

1054

Bouin, M.-N. and Lebeaupin Brossier, C.: Impact of a medicane on the oceanic surface layer from a coupled, kilometre-scale simulation, Ocean Sci., 16, 1125–1142, https://doi.org/10.5194/os-16-1125-2020, 2020.

1055

1056 Catto, J. L. and Dowdy, A.: Understanding compound hazards from a weather system perspective, 1057 Weather and Climate Extremes, 32, 100313, https://doi.org/10.1016/j.wace.2021.100313, 2021.

1058

1059 Chaboureau, J., Pantillon, F., Lambert, D., Richard, E., and Claud, C.: Tropical transition of a 1060 Mediterranean storm by jet crossing, Quart J Royal Meteoro Soc, https://doi.org/10.1002/qj.960, 2012.

1061 1062 1063

1064

Couto, F. T., Kartsios, S., Lacroix, M., and Andrade, H. N.: A Quick Look at the Atmospheric Circulation Leading to Extreme Weather Phenomena on a Continental Scale, Atmosphere, 15, 1205, https://doi.org/10.3390/atmos15101205, 2024.

1065 1066 1067

Davolio, S., Della Fera, S., Laviola, S., Miglietta, M. M., and Levizzani, V.: Heavy Precipitation over Italy from the Mediterranean Storm "Vaia" in October 2018: Assessing the Role of an Atmospheric River, Monthly Weather Review, 148, 3571–3588, https://doi.org/10.1175/MWR-D-20-0021.1, 2020.

1069 1070

1068

1071 De Vries, A. J.: A global climatological perspective on the importance of Rossby wave breaking and 1072 intense moisture transport for extreme precipitation events, Weather Clim. Dynam., 2, 129–161, 1073 https://doi.org/10.5194/wcd-2-129-2021, 2021.

1074

1075 Dente, E., Armon, M., and Shmilovitz, Y.: The September 2023 flood in Derna, Libya: an extreme 1076 weather event or man-made disaster?, EGU General Assembly 2024, Vienna, Austria, 14-19 Apr 1077 https://doi.org/10.5194/egusphere-egu24-15755, EGU24-15755, 2024,

1079 Di Muzio, E., Riemer, M., Fink, A. H., and Maier-Gerber, M.: Assessing the predictability of 1080 Medicanes in ECMWF ensemble forecasts using an object-based approach, Quart J Royal Meteoro 1081 Soc, 145, 1202–1217, https://doi.org/10.1002/qj.3489, 2019.

1082

1083 Dimitriou, E., Efstratiadis, A., Zotou, I., Papadopoulos, A., Iliopoulou, T., Sakki, G.-K., Mazi, K., 1084 Rozos, E., Koukouvinos, A., Koussis, A. D., Mamassis, N., and Koutsoyiannis, D.: Post-Analysis of 1085 Daniel Extreme Flood Event in Thessaly, Central Greece: Practical Lessons and the Value of State-of-1086 the-Art Water-Monitoring Networks, Water, 16, 980, https://doi.org/10.3390/w16070980, 2024.

1087

1088 Faranda, D., Messori, G., and Yiou, P.: Dynamical proxies of North Atlantic predictability and 1089 extremes, Sci Rep, 7, 41278, https://doi.org/10.1038/srep41278, 2017.

1090

- 1091 Faranda, D., Bourdin, S., Ginesta, M., Krouma, M., Noyelle, R., Pons, F., Yiou, P., and Messori, G.:
- 1092 A climate-change attribution retrospective of some impactful weather extremes of 2021, Weather
- 1093 Clim. Dynam., 3, 1311–1340, https://doi.org/10.5194/wcd-3-1311-2022, 2022.

Faranda, D., Ginesta, M., Alberti, T., Coppola, E., and Anzidei, M.: Attributing Venice Acqua Alta events to a changing climate and evaluating the efficacy of MoSE adaptation strategy, npj Clim Atmos Sci, 6, 181, https://doi.org/10.1038/s41612-023-00513-0, 2023a.

1098

Faranda, D., Messori, G., Coppola, E., Alberti, T., Vrac, M., Pons, F., Yiou, P., Saint Lu, M., Hisi, A.
N. S., Brockmann, P., Dafis, S., Mengaldo, G., and Vautard, R.: ClimaMeter: contextualizing extreme
weather in a changing climate, Weather Clim. Dynam., 5, 959–983, https://doi.org/10.5194/wcd-5959-2024, 2024.

1103

1104 Ferrarin, C., Pantillon, F., Davolio, S., Bajo, M., Miglietta, M. M., Avolio, E., Carrió, D. S., Pytharoulis, I., Sanchez, C., Patlakas, P., González-Alemán, J. J., and Flaounas, E.: Assessing the coastal hazard of Medicane Ianos through ensemble modelling, Nat. Hazards Earth Syst. Sci., 23, 1107 2273–2287, https://doi.org/10.5194/nhess-23-2273-2023, 2023a.

1108

1109 Ferrarin, C., Orlić, M., Bajo, M., Davolio, S., Umgiesser, G., and Lionello, P.: The contribution of a
1110 mesoscale cyclone and associated meteotsunami to the exceptional flood in Venice on November 12,
1111 2019, Quart J Royal Meteoro Soc, 149, 2929–2942, https://doi.org/10.1002/qj.4539, 2023b.

1112

Flaounas, E., Raveh-Rubin, S., Wernli, H., Drobinski, P., and Bastin, S.: The dynamical structure of intense Mediterranean cyclones, Clim Dyn, 44, 2411–2427, https://doi.org/10.1007/s00382-014-2330-2, 2015.

1116

Flaounas, E., Di Luca, A., Drobinski, P., Mailler, S., Arsouze, T., Bastin, S., Beranger, K., and Lebeaupin Brossier, C.: Cyclone contribution to the Mediterranean Sea water budget, Clim Dyn, 46, 913–927, https://doi.org/10.1007/s00382-015-2622-1, 2016.

1120

1121 Flaounas, E., Kotroni, V., Lagouvardos, K., Gray, S. L., Rysman, J.-F., and Claud, C.: Heavy rainfall in Mediterranean cyclones. Part I: contribution of deep convection and warm conveyor belt, Clim Dyn, 50, 2935–2949, https://doi.org/10.1007/s00382-017-3783-x, 2018.

1124

Flaounas, E., Fita, L., Lagouvardos, K., and Kotroni, V.: Heavy rainfall in Mediterranean cyclones, Part II: Water budget, precipitation efficiency and remote water sources, Clim Dyn, 53, 2539–2555, https://doi.org/10.1007/s00382-019-04639-x, 2019.

1128

Flaounas, E., Gray, S. L., and Teubler, F.: A process-based anatomy of Mediterranean cyclones: from baroclinic lows to tropical-like systems, Weather Clim. Dynam., 2, 255–279, https://doi.org/10.5194/wcd-2-255-2021, 2021.

1132

Flaounas, E., Davolio, S., Raveh-Rubin, S., Pantillon, F., Miglietta, M. M., Gaertner, M. A., Hatzaki,
M., Homar, V., Khodayar, S., Korres, G., Kotroni, V., Kushta, J., Reale, M., and Ricard, D.:
Mediterranean cyclones: current knowledge and open questions on dynamics, prediction, climatology
and impacts, Weather Clim. Dynam., 3, 173–208, https://doi.org/10.5194/wcd-3-173-2022, 2022.

1137

Flaounas, E., Aragão, L., Bernini, L., Dafis, S., Doiteau, B., Flocas, H., Gray, S. L., Karwat, A., Kouroutzoglou, J., Lionello, P., Miglietta, M. M., Pantillon, F., Pasquero, C., Patlakas, P., Picornell, M. Á., Porcù, F., Priestley, M. D. K., Reale, M., Roberts, M. J., Saaroni, H., Sandler, D., Scoccimarro, E., Sprenger, M., and Ziv, B.: A composite approach to produce reference datasets for extratropical cyclone tracks: application to Mediterranean cyclones, Weather Clim. Dynam., 4, 639–661,

11431144

1145 Grimaldi, S., Salamon, P., Disperati, J., Zsoter, E., Russo, C., Ramos, A., Carton De Wiart, C.,

https://doi.org/10.5194/wcd-4-639-2023, 2023.

- 1146 Barnard, C., Hansford, E., Gomes, G., Prudhomme, C. (2022): River discharge and related historical
- 1147 data from the Global Flood Awareness System. v4.0. European Commission, Joint Research Centre
- 1148 (JRC). URL: https://cds.climate.copernicus.eu/cdsapp#!/dataset/cems-glofas-historical (Accessed on

1149 09-Oct-2023)

1150

1151 Global Data Institute of the UN International Organization for Migration (IOM), 2023. Libya —

1152 Storm Daniel Flash update 3 (14 September 2023)

1153

1154 He, K., Yang, Q., Shen, X., Dimitriou, E., Mentzafou, A., Papadaki, C., Stoumboudi, M., and 1155 Anagnostou, E. N.: Brief communication: Storm Daniel Flood Impact in Greece 2023: Mapping Crop

1156 and Livestock Exposure from SAR, https://doi.org/10.5194/nhess-2023-173, 12 October 2023.

1157

- 1158 Hersbach, H., Bell, B., Berrisford, P., Hirahara, S., Horányi, A., Muñoz-Sabater, J., Nicolas, J.,
- Peubey, C., Radu, R., Schepers, D., Simmons, A., Soci, C., Abdalla, S., Abellan, X., Balsamo, G., 1159
- 1160 Bechtold, P., Biavati, G., Bidlot, J., Bonavita, M., De Chiara, G., Dahlgren, P., Dee, D., Diamantakis, M., Dragani, R., Flemming, J., Forbes, R., Fuentes, M., Geer, A., Haimberger, L., Healy, S., Hogan, 1161
- 1162 R. J., Hólm, E., Janisková, M., Keeley, S., Laloyaux, P., Lopez, P., Lupu, C., Radnoti, G., De Rosnay,
- 1163 P., Rozum, I., Vamborg, F., Villaume, S., and Thépaut, J.: The ERA5 global reanalysis, Quart J Royal
- 1164 Meteoro Soc, 146, 1999–2049, https://doi.org/10.1002/qj.3803, 2020.

1165

- 1166 Hewson, T., Ashoor, A., Boussetta, S., Emanuel, K., Lagouvardos, K., Lavers, D., Magnusson, L.,
- 1167 Pillosu, F., Zsoter, E., Medicane Daniel: an extraordinary cyclone with devastating impacts, ECMWF
- 1168 newsletters 179, 2024, 33-47.

1169

- 1170 Hochman, A., Scher, S., Quinting, J., Pinto, J. G., and Messori, G.: Dynamics and predictability of
- 1171 2047-2064, over the Eastern Mediterranean, Clim Dyn, 58,
- 1172 https://doi.org/10.1007/s00382-020-05465-2, 2022a.

1173

- 1174 Hochman, A., Marra, F., Messori, G., Pinto, J. G., Raveh-Rubin, S., Yosef, Y., and Zittis, G.: Extreme
- 1175 weather and societal impacts in the eastern Mediterranean, Earth Syst. Dynam., 13, 749–777,
- 1176 https://doi.org/10.5194/esd-13-749-2022, 2022b.

1177

1178 Hochman, A., Plotnik, T., Marra, F., Shehter, E.-R., Raveh-Rubin, S., and Magaritz-Ronen, L.: The 1179 sources of extreme precipitation predictability; the case of the 'Wet' Red Sea Trough, Weather and 1180 Climate Extremes, 40, 100564, https://doi.org/10.1016/j.wace.2023.100564, 2023.

1181

- Hochman, A., Shachar, N., and Gildor, H.: Unraveling sub-seasonal precipitation variability in the 1182 1183 East via Indian Ocean sea surface temperature, Sci
- 1184 https://doi.org/10.1038/s41598-024-53677-x, 2024.

1185

- 1186 IFRC (International Federation of Red Cross and Red Crescent Societies). World Disasters Report
- 1187 2020 Executive Summary. https://www.ifrc.org/document/world-disasters-report-2020

1188

- 1189 Khodayar, S., Davolio, S., Di Girolamo, P., Lebeaupin Brossier, C., Flaounas, E., Fourrie, N., Lee,
- 1190 K.-O., Ricard, D., Vie, B., Bouttier, F., Caldas-Alvarez, A., and Ducrocq, V.: Overview towards
- 1191 improved understanding of the mechanisms leading to heavy precipitation in the western 1192 Mediterranean: lessons learned from HyMeX, Atmos. Chem. Phys., 21, 17051–17078,
- 1193 https://doi.org/10.5194/acp-21-17051-2021, 2021.

1194

- 1195 Korres, G., Ravdas, M., Denaxa, D., & Sotiropoulou, M. (2021). Mediterranean Sea Waves
- 1196 Reanalysis INTERIM (CMEMS Med-Waves, MedWAM3I system) (Version 1) [Data set].
- 1197 Copernicus Monitoring Environment Marine Service (CMEMS).
- 1198 https://doi.org/10.25423/CMCC/MEDSEA_MULTIYEAR_WAV_006_012_MEDWAM3I

1199

1200 Korres, G., Oikonomou, C., Denaxa, D., & Sotiropoulou, M. (2023). Mediterranean Sea Waves

- Analysis and Forecast (Copernicus Marine Service MED-Waves, MEDWAM4 system) (Version 1) [Data set]. Copernicus Marine Service (CMS).
- 1203 https://doi.org/10.25423/CMCC/MEDSEA_ANALYSISFORECAST_WAV_006_017_MEDWAM4

Lagouvardos, K., Kotroni, V., Bezes, A., Koletsis, I., Kopania, T., Lykoudis, S., Mazarakis, N., Papagiannaki, K., and Vougioukas, S.: The automatic weather stations NOANN network of the National Observatory of Athens: operation and database, Geoscience Data Journal, 4, 4–16, https://doi.org/10.1002/gdj3.44, 2017.

Messmer, M., Gómez-Navarro, J. J., and Raible, C. C.: Sensitivity experiments on the response of Vb cyclones to sea surface temperature and soil moisture changes, Earth Syst. Dynam., 8, 477–493, https://doi.org/10.5194/esd-8-477-2017, 2017.

Miglietta, M. M., Moscatello, A., Conte, D., Mannarini, G., Lacorata, G., and Rotunno, R.: Numerical analysis of a Mediterranean 'hurricane' over south-eastern Italy: Sensitivity experiments to sea surface temperature, Atmospheric Research, 101, 412–426, https://doi.org/10.1016/j.atmosres.2011.04.006, 2011.

Miglietta, M. M., Carnevale, D., Levizzani, V., and Rotunno, R.: Role of moist and dry air advection
in the development of Mediterranean tropical-like cyclones (medicanes), Quart J Royal Meteoro Soc,
147, 876–899, https://doi.org/10.1002/qj.3951, 2021.

Miglietta M. M., González-Alemán J. J., Panegrossi G., Gaertner M. A., Pantillon F., Pasquero C., Schultz D. M., D'Adderio L. P., Dafis S., Husson R., Ricchi A., Carrió D. S., Davolio S., Fita L., Picornell M. A., Pytharoulis I., Raveh-Rubin S., Scoccimarro E., Bernini L., Cavicchia L., Conte D., Ferretti R., Flocas H., Gutiérrez-Fernández J., Hatzaki M., Homar Santaner V., Jansà A., Patlakas P., Flaounas E., Defining Medicanes: Bridging the Knowledge Gap Between Tropical and Extratropical Cyclones in the Mediterranean, Bull. Am. Meteor. Soc., submitted

Nissen, K. M., Leckebusch, G. C., Pinto, J. G., Renggli, D., Ulbrich, S., and Ulbrich, U.: Cyclones causing wind storms in the Mediterranean: characteristics, trends and links to large-scale patterns, Nat. Hazards Earth Syst. Sci., 10, 1379–1391, https://doi.org/10.5194/nhess-10-1379-2010, 2010.

Pantillon, F. P., Chaboureau, J.-P., Mascart, P. J., and Lac, C.: Predictability of a Mediterranean Tropical-Like Storm Downstream of the Extratropical Transition of Hurricane Helene (2006), Monthly Weather Review, 141, 1943–1962, https://doi.org/10.1175/MWR-D-12-00164.1, 2013.

Pantillon, F., Davolio, S., Avolio, E., Calvo-Sancho, C., Carrió, D. S., Dafis, S., Gentile, E. S., Gonzalez-Aleman, J. J., Gray, S., Miglietta, M. M., Patlakas, P., Pytharoulis, I., Ricard, D., Ricchi, A., Sanchez, C., and Flaounas, E.: The crucial representation of deep convection for the cyclogenesis of Medicane Ianos, Weather Clim. Dynam., 5, 1187–1205, https://doi.org/10.5194/wcd-5-1187-2024, 2024. Pantillon, F., Davolio, S., Avolio, E., Calvo-Sancho, C., Carrió, D. S., Dafis, S., Flaounas, E., Gentile, E. S., Gonzalez-Aleman, J. J., Gray, S., Miglietta, M. M., Patlakas, P., Pytharoulis, I., Ricard, D., Ricchi, A., and Sanchez, C.: The crucial representation of deep convection for the cyclogenesis of medicane Ianos, https://doi.org/10.5194/egusphere-2024-1105, 7 May 2024.

Patlakas, P., Stathopoulos, C., Tsalis, C., and Kallos, G.: Wind and wave extremes associated with tropical-like cyclones in the Mediterranean basin, Intl Journal of Climatology, 41, https://doi.org/10.1002/joc.6795, 2021.

Pfahl, S. and Wernli, H.: Quantifying the Relevance of Cyclones for Precipitation Extremes, Journal of Climate, 25, 6770–6780, https://doi.org/10.1175/JCLI-D-11-00705.1, 2012.

Portal, A., Raveh-Rubin, S., Catto, J. L., Givon, Y., and Martius, O.: Linking compound weather extremes to Mediterranean cyclones, fronts, and airstreams, Weather Clim. Dynam., 5, 1043–1060,

1263

1281

1286 1287

1288

1289

1290 1291

1292

1295

1296

1309

- 1256 https://doi.org/10.5194/wcd-5-1043-2024, 2024.Portal, A., Raveh-Rubin, S., Catto, J. L., Givon, Y., 1257 and Martius, O.: Linking compound weather extremes to Mediterranean cyclones, fronts and air-1258 streams, https://doi.org/10.5194/egusphere-2024-270, 8 February 2024.
- 1260 Pytharoulis, I.: Analysis of a Mediterranean tropical-like cyclone and its sensitivity to the sea surface 1261 temperatures, Atmospheric Research, 208, 167–179, https://doi.org/10.1016/j.atmosres.2017.08.009, 1262 2018.
- 1264 Qiu J., Zhao W., Brocca L., Paolo Tarolli (2023). Storm Daniel revealed the fragility of the 1265 Mediterranean region. The Innovation Geoscience 1(3), 100036. https://doi.org/10.59717/j.xinn-1266 geo.2023.100036 1267
- 1268 Raveh-Rubin, S. and Flaounas, E.: A dynamical link between deep Atlantic extratropical cyclones and 1269 Mediterranean cyclones, Atmospheric Science Letters, 18, 215-221, 1270 https://doi.org/10.1002/asl.745, 2017. 1271
- 1272 Raveh-Rubin, S. and Wernli, H.: Large-scale wind and precipitation extremes in the Mediterranean: 1273 dynamical aspects of five selected cyclone events, Quart J Royal Meteoro Soc, 142, 3097-3114, 1274 https://doi.org/10.1002/qj.2891, 2016. 1275
- 1276 Reale, M., Cabos Narvaez, W. D., Cavicchia, L., Conte, D., Coppola, E., Flaounas, E., Giorgi, F., 1277 Gualdi, S., Hochman, A., Li, L., Lionello, P., Podrascanin, Z., Salon, S., Sanchez-Gomez, E., 1278 Scoccimarro, E., Sein, D. V., and Somot, S.: Future projections of Mediterranean cyclone 1279 characteristics using the Med-CORDEX ensemble of coupled regional climate system models, Clim 1280 Dyn, 58, 2501–2524, https://doi.org/10.1007/s00382-021-06018-x, 2022.
- 1282 Ricchi, A., Miglietta, M. M., Barbariol, F., Benetazzo, A., Bergamasco, A., Bonaldo, D., Cassardo, C., 1283 Falcieri, F. M., Modugno, G., Russo, A., Sclavo, M., and Carniel, S.: Sensitivity of a Mediterranean 1284 tropical-like cyclone to different model configurations and coupling strategies, Atmosphere, 8, 1–32, 1285 https://doi.org/10.3390/atmos8050092, 2017.
 - Romero, R. and Emanuel, K.: Climate Change and Hurricane-Like Extratropical Cyclones: Projections for North Atlantic Polar Lows and Medicanes Based on CMIP5 Models, J. Climate, 30, 279–299, https://doi.org/10.1175/JCLI-D-16-0255.1, 2017.
- Rousseau-Rizzi, R., Raveh-Rubin, S., Catto, J. L., Portal, A., Givon, Y., and Martius, O.: A stormrelative climatology of compound hazards in Mediterranean cyclones, Weather Clim. Dynam., 5, 1293 1079–1101, https://doi.org/10.5194/wcd-5-1079-2024, 2024. Rousseau-Rizzi, R., Raveh-Rubin, S., 1294 Catto, J., Portal, A., Givon, Y., and Martius, O.: A storm-relative climatology of compound hazards in Mediterranean cyclones, https://doi.org/10.5194/egusphere-2023-2322, 17 October 2023.
- 1297 Sanchez, C., Gray, S., Volonte', A., Pantillon, F., Berthou, S., and Davolio, S.: The impact of 1298 preceding convection on the development of Medicane Ianos and the sensitivity to sea surface 1299 temperature. Weather Clim. Dynam., 5, 1429 - 1455, https://doi.org/10.5194/wcd-5-1429-2024, 2024. 1300
- 1301 Scherrmann, A., Wernli, H., and Flaounas, E.: The upstream-downstream connection of North 1302 Atlantic and Mediterranean cyclones in semi-idealized simulations, Weather Clim. Dynam., 5, 419-1303 438, https://doi.org/10.5194/wcd-5-419-2024, 2024. 1304
- 1305 Shirzaei, M., Vahedifard, F., Sadhasivam, N., Ohenhen, L., Dasho, O., Tiwari, A., Werth, S., Azhar, 1306 M., Zhao, Y., Nicholls, R. J., and AghaKouchak, A.: Aging dams, political instability, poor human 1307 decisions and climate change: recipe for human disaster, npj Nat. Hazards, 2, 1-8, 1308 https://doi.org/10.1038/s44304-024-00056-1, 2025.

- 1310 Sioni, F., Davolio, S., Grazzini, F., and Giovannini, L.: Revisiting the atmospheric dynamics of the two century floods over north-eastern Italy. Atmos. Research, 286, 106662, https://doi.org/10.1016/j.atmosres.2023.106662, 2023.
- 1313 |
 1314 Sodemann, H., Schwierz, C., and Wernli, H.: Interannual variability of Greenland winter precipitation sources: Lagrangian moisture diagnostic and North Atlantic Oscillation influence, J. Geophys. Res.,
 1316 13, 2007JD008503, https://doi.org/10.1029/2007JD008503, 2008.
- 1317
 1318 Sprenger, M. and Wernli, H.: The LAGRANTO Lagrangian analysis tool version 2.0, Geosci.
 1319 Model Dev., 8, 2569–2586, https://doi.org/10.5194/gmd-8-2569-2015, 2015.
- 1321 UNICEF. 2023. Libya Storm Daniel & Flooding, Situation Report #1. (14-09-2023) 1322
- United Nations Office for the Coordination of Humanitarian Affairs (OCHA). 2023. Flash Appeal
 Libya.
 1325
- 1326 Varlas, G., Vervatis, V., Spyrou, C., Papadopoulou, E., Papadopoulos, A., and Katsafados, P.: Investigating the impact of atmosphere—wave—ocean interactions on a Mediterranean tropical-like cyclone, Ocean Model., 153, 101675, https://doi.org/10.1016/j.ocemod.2020.101675, 2020.
 1329 Varlas, G., Vervatis, V., Spyrou, C., Papadopoulou, E., Papadopoulos, A., and Katsafados, P.: Investigating the impact of atmosphere—wave—ocean interactions on a Mediterranean tropical-like cyclone, Ocean Model., 153, 101675, https://doi.org/10.1016/j.ocemod.2020.101675, 2020.
- 1330 | Vito Romaniello, Paolo Oddo, Marina Tonani, Lucio Torrisi, Alessandro Grandi, and Nadia Pinardi:
 1331 | Impact of Sea Surface Temperature on COSMO Forecasts of a Medicane over the Western
 1332 | Mediterranean Sea, JEASE, 5, https://doi.org/10.17265/2159-581X/2015.06.002, 2015.
 1333 | Vito Romaniello, Paolo Oddo, Marina Tonani, Lucio Torrisi, Alessandro Grandi, and Nadia Pinardi:
 1331 | Mediterranean Sea, JEASE, 5, https://doi.org/10.17265/2159-581X/2015.06.002, 2015.
- 1334 Weather Meteorological Organisation: https://wmo.int/media/news/libya-floods-show-need-multi 1335 hazard-early-warnings-unified-response, last access: 10 March 2024.
 1336 hazard-early-warnings-unified-response, last access: 10 March 2024.
- Weather Meteorological Organisation: https://wmo.int/media/news/storm-daniel-leads-extreme-rain-and-floods-mediterranean-heavy-loss-of-life-libya, last access: 3 February, 2025
 1339
- Wernli, H. and Davies, H. C.: A Lagrangian-based analysis of extratropical cyclones. I: The method and some applications, Quart J Royal Meteoro Soc, 123, 467–489, https://doi.org/10.1002/qj.49712353811, 1997.
- World Bank, 2023. Libya Storm and Flooding 2023. Rapid Damage and Needs Assessment.
 Washington, DC: World Bank, http://recovery.preventionweb.net/quick/82808.
 1346

Figures

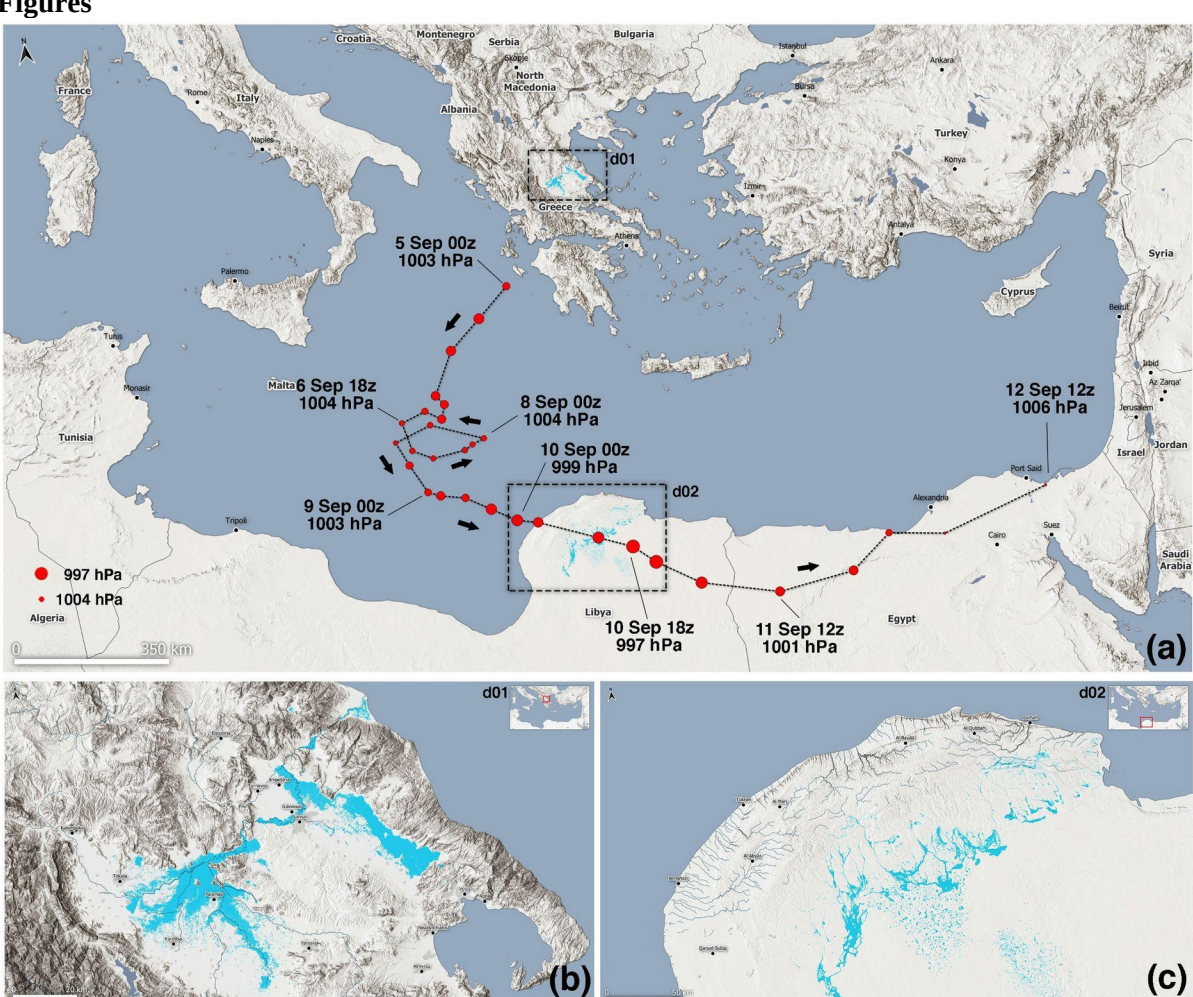


Figure 1 (a) Track of <u>Storm</u> Daniel <u>storm atim six-hourly intervals</u>; <u>based on ECMWF analysis</u>, where the size of red dots is proportional to cyclone depth in terms of minimum mean sea level pressure. Flooded areas are shown in cyan and blue tones (acquired by one of the Copernicus Sentinel-2 satellites on <u>10</u>2 and 12 September <u>2023</u>). Panels **(b)** and **(c)** zoom over central Greece and Libya (square boxes in panel **a**).

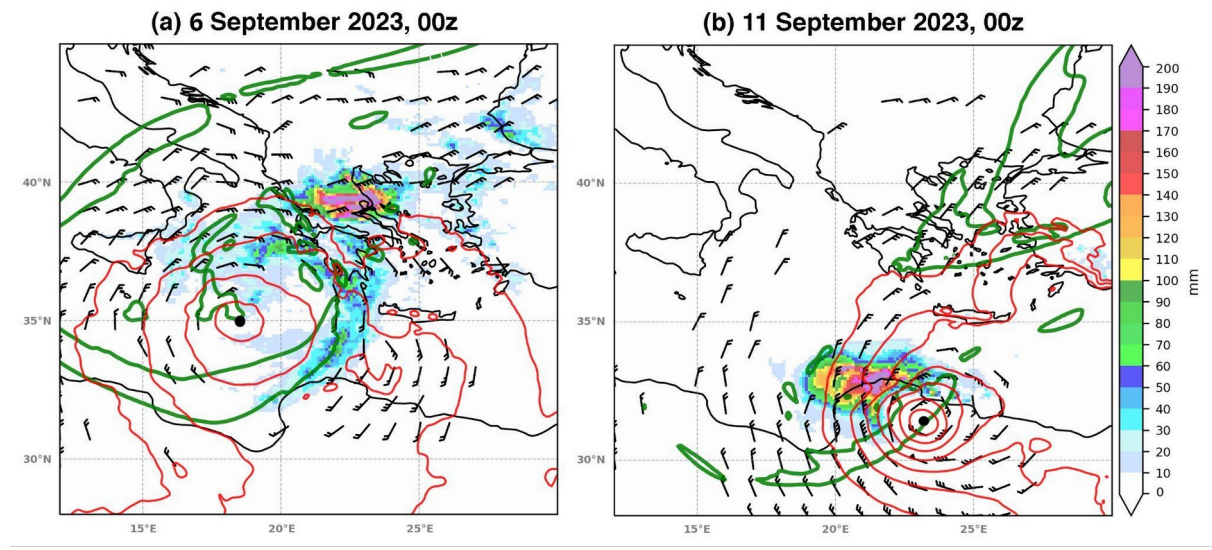


Figure 2 (a) Potential Vorticity of 2 PVU at 300 hPa (in green contour) and wind speed higher than 15 knots at 850 hPa (in barbs, with full and half bars depicting 10 and 5 knots, respectively) and mean sea level pressure (in red contours for values lower than 1012 hPa with 2 hPa interval) on 65 September 5, 2023, at 0012_UTC. 24-hour total accumulated precipitation from 5 to 6 of September 00:00 UTC is shown in shading (max value 434 mm). **(b)** Same as **(a)** but for 11 September 11, 2023, at 00 UTC (max precipitation value 382 mm). The In both panels, the black dot indicates the minimum sea level pressure position in both panels.

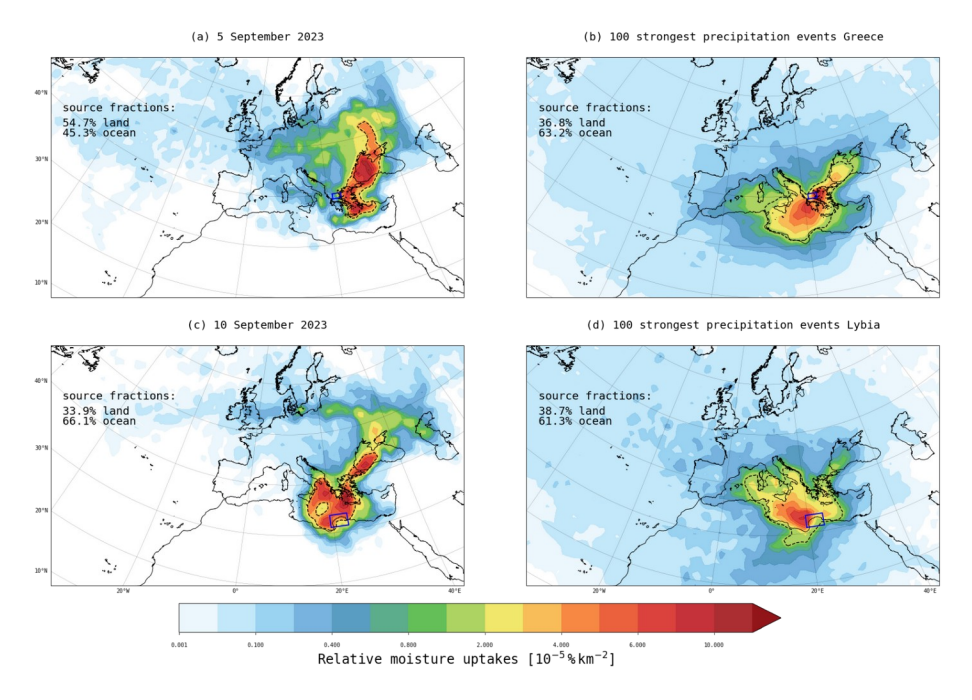


Figure 3 (a) Relative Accumulated moisture uptakes sources that contribute to the precipitation event in Thessaly (depicted withby the blue rectangle) on 5 September 2023. The black dashed contours outlines the largest moisture source regions, which account for 90%, 75%, 50%, and 25% of the total moisture uptake. The numbers onin the top left showgive the relative land and ocean fraction of the moisture sources. (b) as in (a) but for the 100 most extreme daily precipitation events in Thessaly from 1990 to 2023. (c) as in (a) but for the precipitation in the study region in Libya (blue rectangle) on 10 September 2023. (d) as in (be) but for Libya.

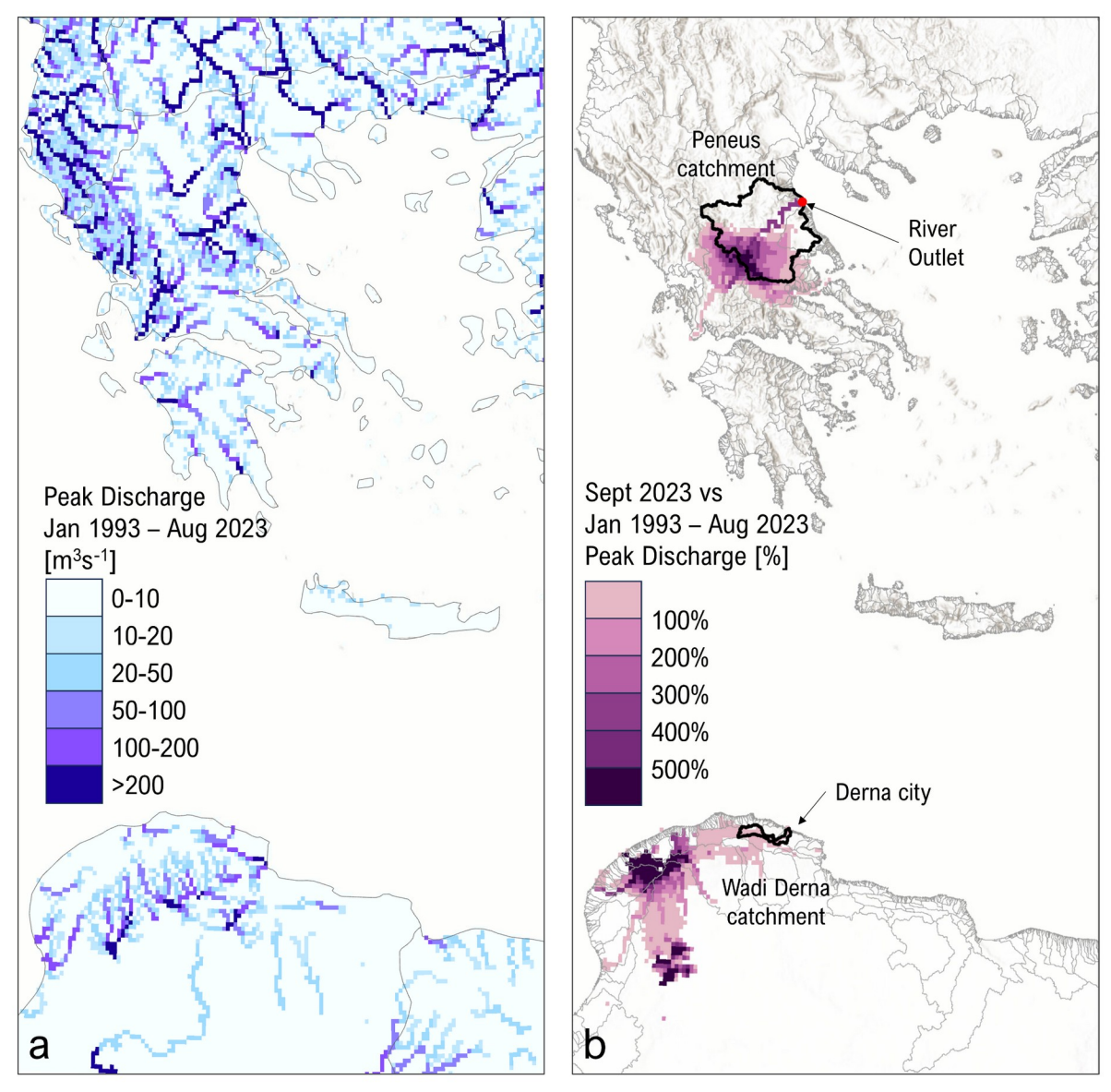


Figure 4 Peak discharge over three recent decades (<u>Jan 1993 – Aug 20231993-2023</u>) versus Daniel storm as represented by the Global Flood Awareness System (**a**) spatial distribution of the maximum peak river discharge from January 1993 to August 2023, (**b**) comparison map for September 2023 illustrating the <u>event-wide</u> peak discharges as a percentage increase over the maximum peak discharges during the 30 years <u>from January 1993 to August 2023</u> in (**a**).

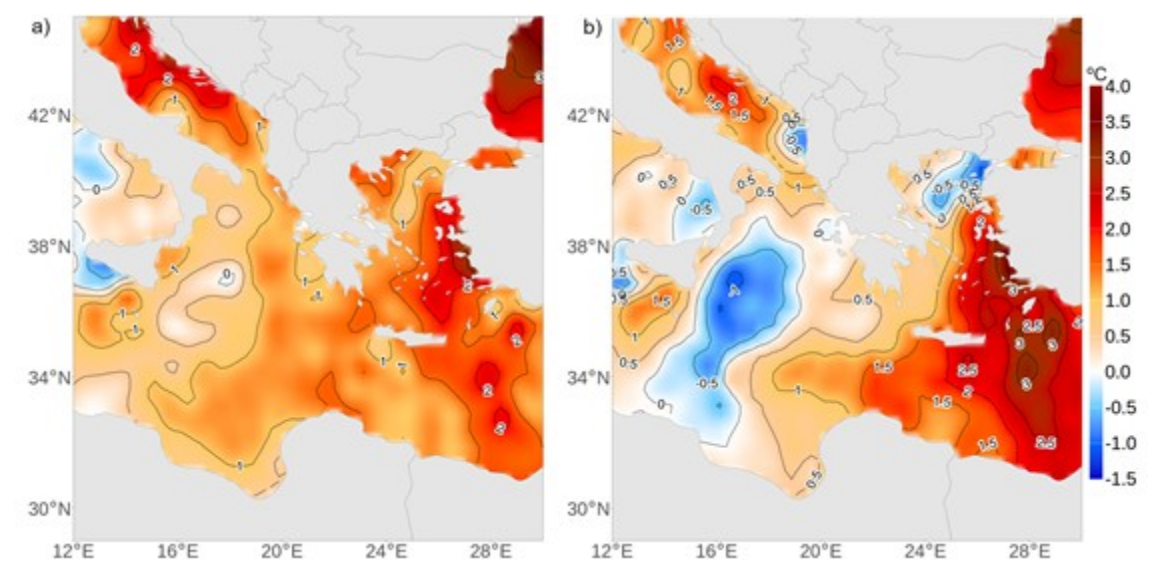


Figure 5 (a) Daily SST anomaly <u>from ERA5</u>, for 3 September 2023, and (b) 9 September 2023. The reference climatology for anomaly determination is 1982-2011.

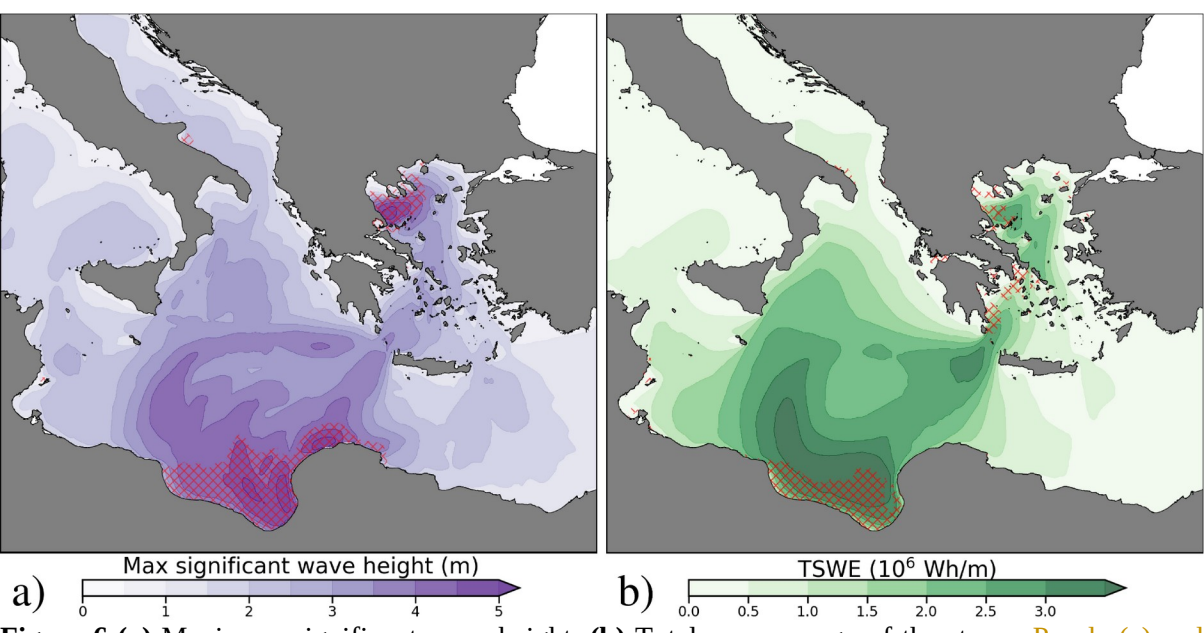


Figure 6 (a) Maximum significant wave height. **(b)** Total wave energy of the storm. <u>Purple (a) and real (b)</u> patches mark areas of extreme conditions (above the 99th percentile) determined based on the Mediterranean Sea wave reanalysis.

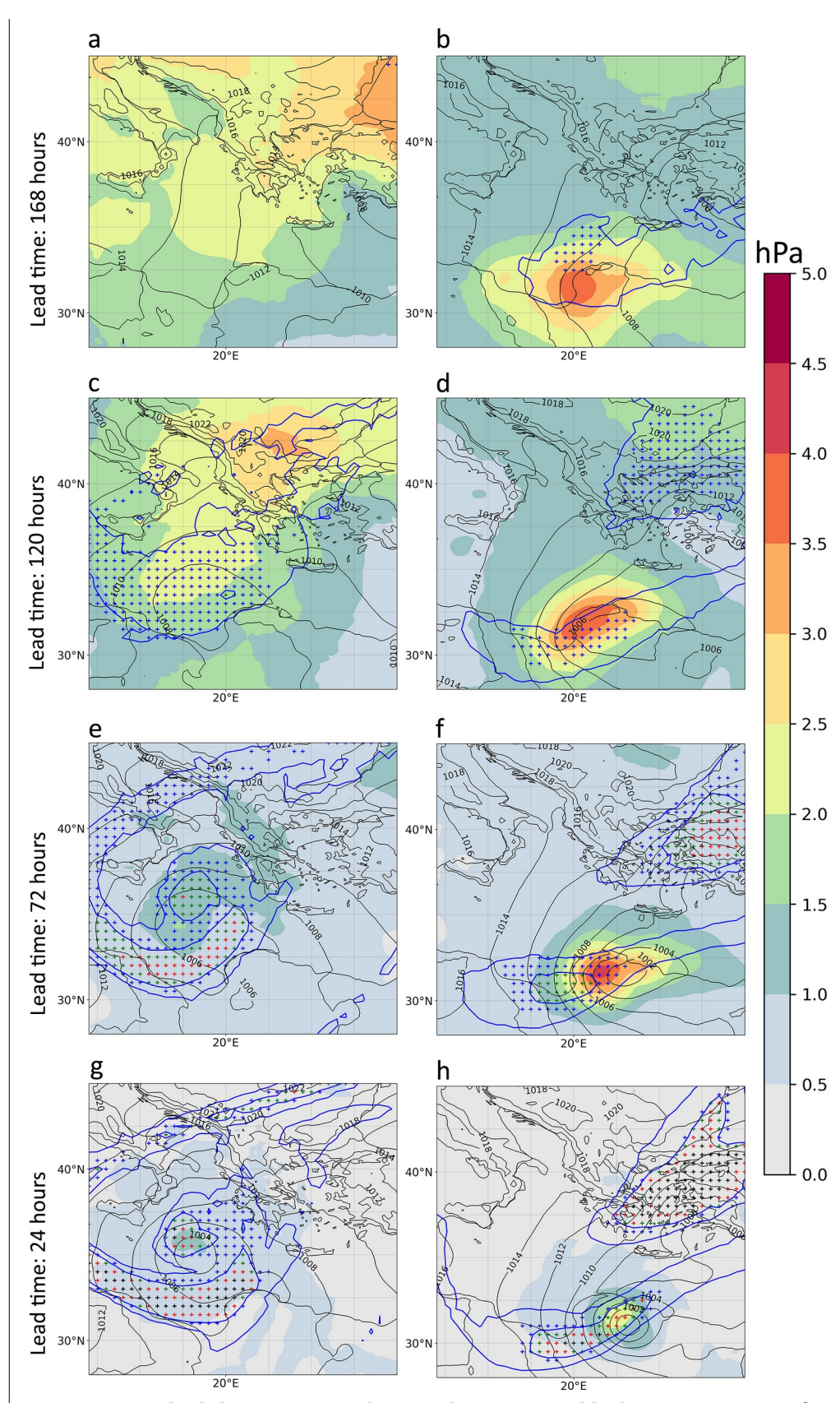


Figure 7 Standard deviation (in colour) and average (in black contour) MSLP from the 51 ensemble members of the ECMWF EPS. Blue contours enclose areas with <u>a median equal toan average of 1</u> and 2 PVU at 300 hPa among all members of the EPS. Blue crosses indicate areas where <u>at leastmore than</u> 25% of the members have PV values greater than 2 PVU. Green, red, and black crosses denote <u>member</u> agreement <u>by at least</u> 50%, 75%, and 95% <u>of the members</u>, respectively. Panels depict

different lead forecast times valid on $5\underline{6}$ September at $\underline{00:0012}$ UTC (panels **a**, **c**, **e**, **g**) and $1\underline{10}$ September at $\underline{00:0012}$ UTC (**b**, **d**, **f**, **h**).

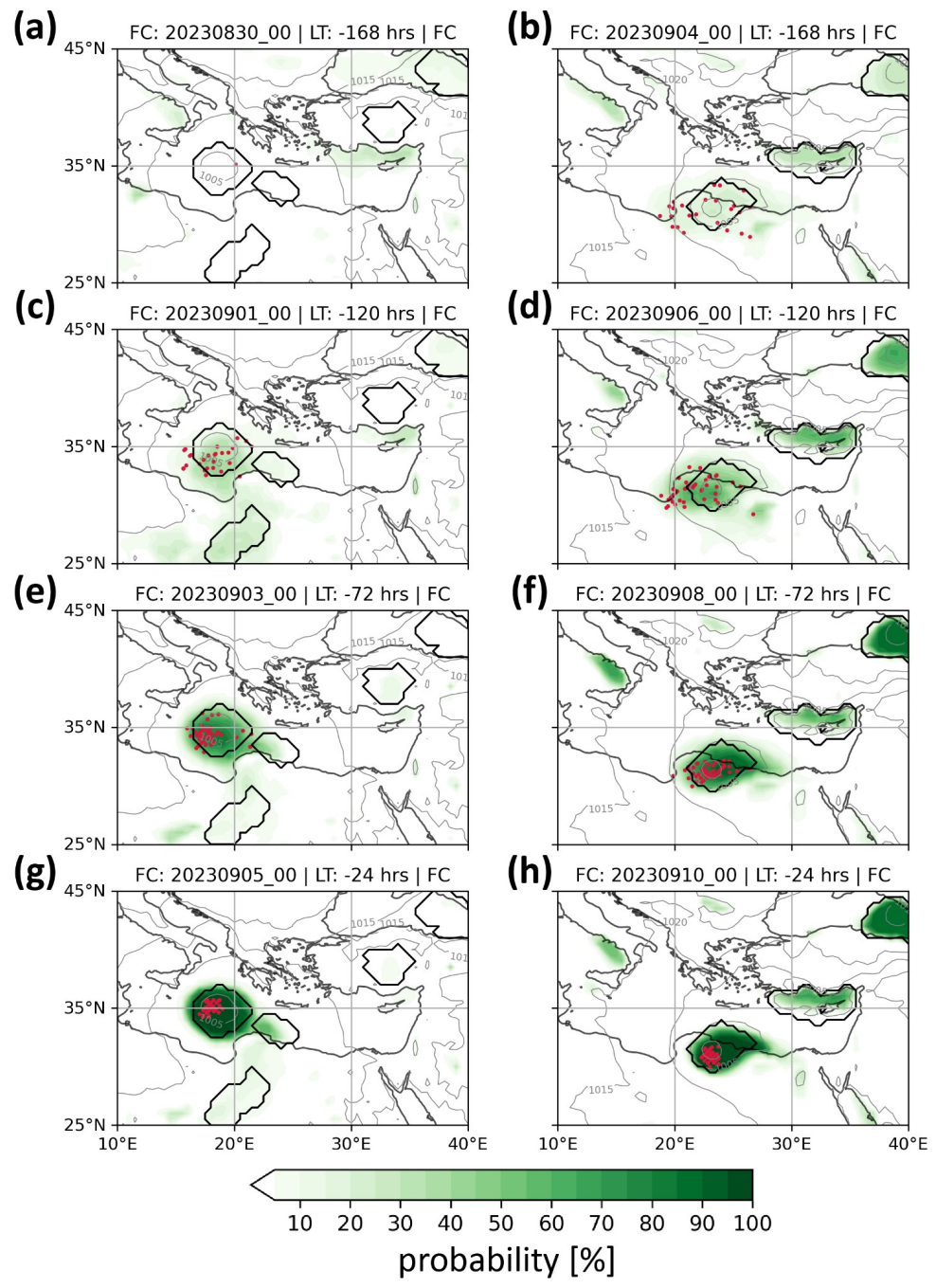


Figure 8 Percentage of overlapping cyclone objects (green shading) among the ensemble prediction system members for different lead times valid on 65 September 2023, 00:1200 UTC (left column panels) and 11 September 2023, 00:00 UTC (right column panels). Black contours show cyclone objects in ECMWF analysis (grey contours for MSLP_isobars in ECMWF analysis). Red dots depict the location of the minimum pressure of Daniel in the ensemble members.

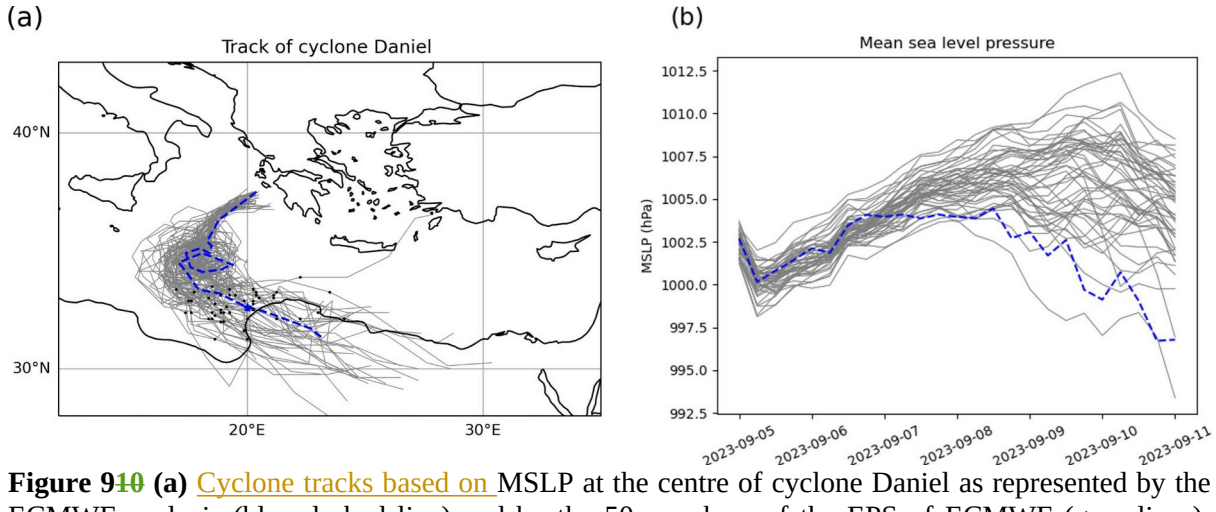


Figure 910 (a) Cyclone tracks based on MSLP at the centre of cyclone Daniel as represented by the ECMWF analysis (blue dashed line) and by the 50 members of the EPS of ECMWF (grey lines), initialized on 54 September at 00:00 UTC. Black dots in (a) depict the cyclone location on 10 September, 00:00 UTC (b) As in (a) but as a time series of minimum MSLP tracks of cyclone Daniel but for tracks of cyclone Daniel.

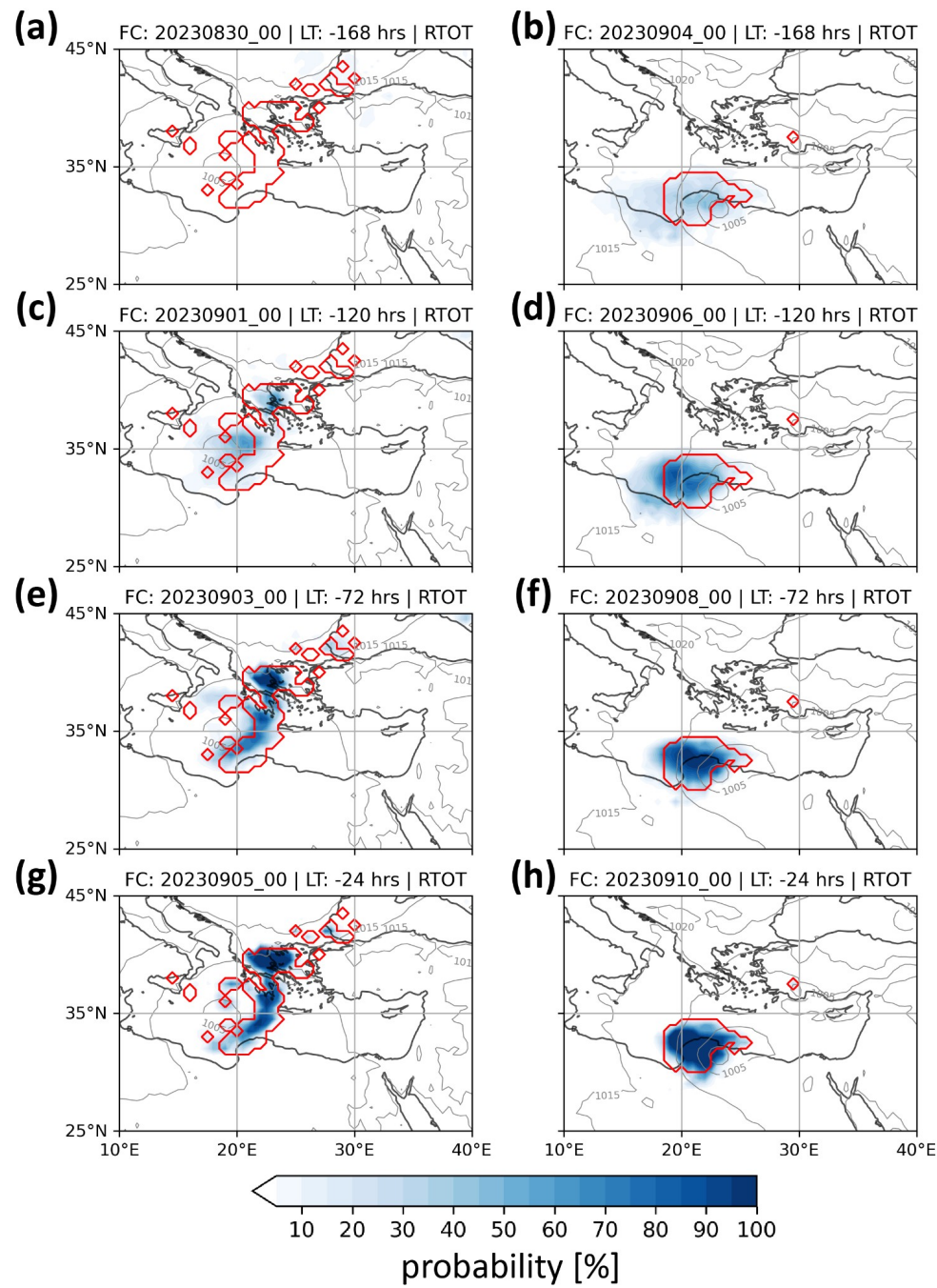
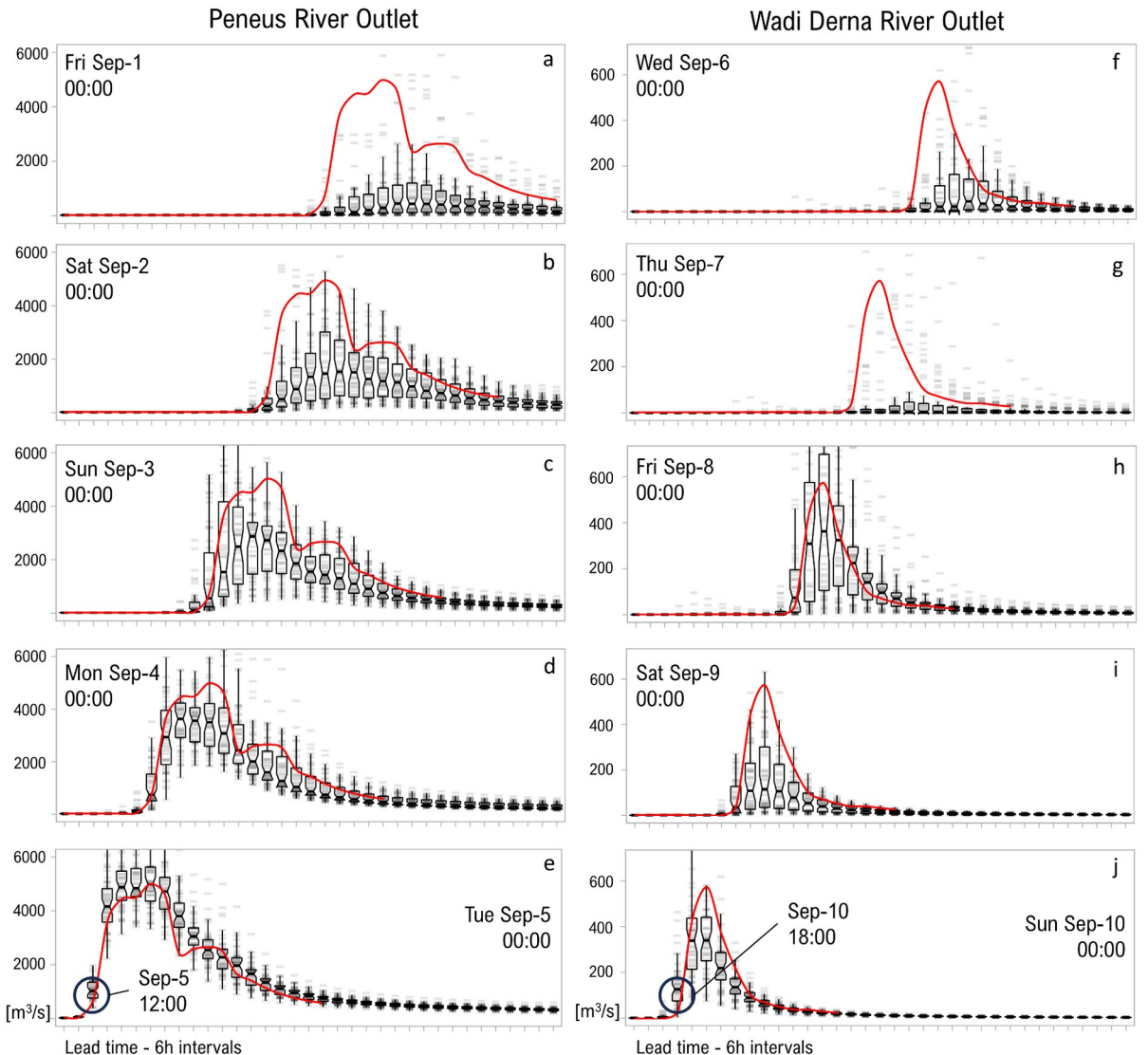


Figure 109 Percentage of overlapping objects (in blue shading) among the ensemble prediction members for 24-hour accumulation (ending at the validity time) of extreme precipitation for different lead times valid on 65 September 2023, 00:1200 UTC (left column panels) and 11 September 2023, 00:00 UTC (right column panels). Red contours show objects of extreme precipitation determined based on an ERA5 climatology (grey contours for MSLP isobars in ECMWF analysis).



1461 1462 1463 1464 1465 1466 1467 1468 1469 1470 1471 1472 1473 1474 1475 1476 1477

Fig 11 Six-hourly ensemble river discharge forecasts forecasts of river discharge for the Peneus and Wadi Derna catchments compared to the "perfect forecast" benchmark (red line). The "perfect forecast" represents the initialization of each forecast for all time steps across the event, as taken as a reference for evaluating forecast accuracy... wiWithth the observed timing of rising hydrograph limbs marked on 5 September 5th, 12noon :00 PM local time (09 UTC) for the Peneus River in Thessaly, and 10 September-10th, 18:00 local time (16 UTC) for the Wadi Derna River. Grey stripes (tick marks) representrepresenting individual ensemble members from the EFAS model, driven by the 51 ensemble members of the ECMWF EPS. Overlapping tick marks darken, visually highlighting areas of member agreement (convergence). Forecast summary data are displayed as boxplots, where the box represents the interquartile range (IQR), the whiskers show the range of values within 1.5 times the IQR, and the horizontal black line inside the box indicates the median. The notches around the median shows the 95% confidence interval. Six-hourly ensemble forecasts of river discharge by the European Flood Awareness System, shown for different lead times. The red line represents the 'perfect forecast' benchmark, with the observed timing of rising hydrograph limbs marked on September 5th, 12:00 PM local time for the PeneusPineios River in Thessaly, and September 10th, 18:00 local time for the Wandi Derna River. Box plots and grey lines indicate individual ensemble member predictions.

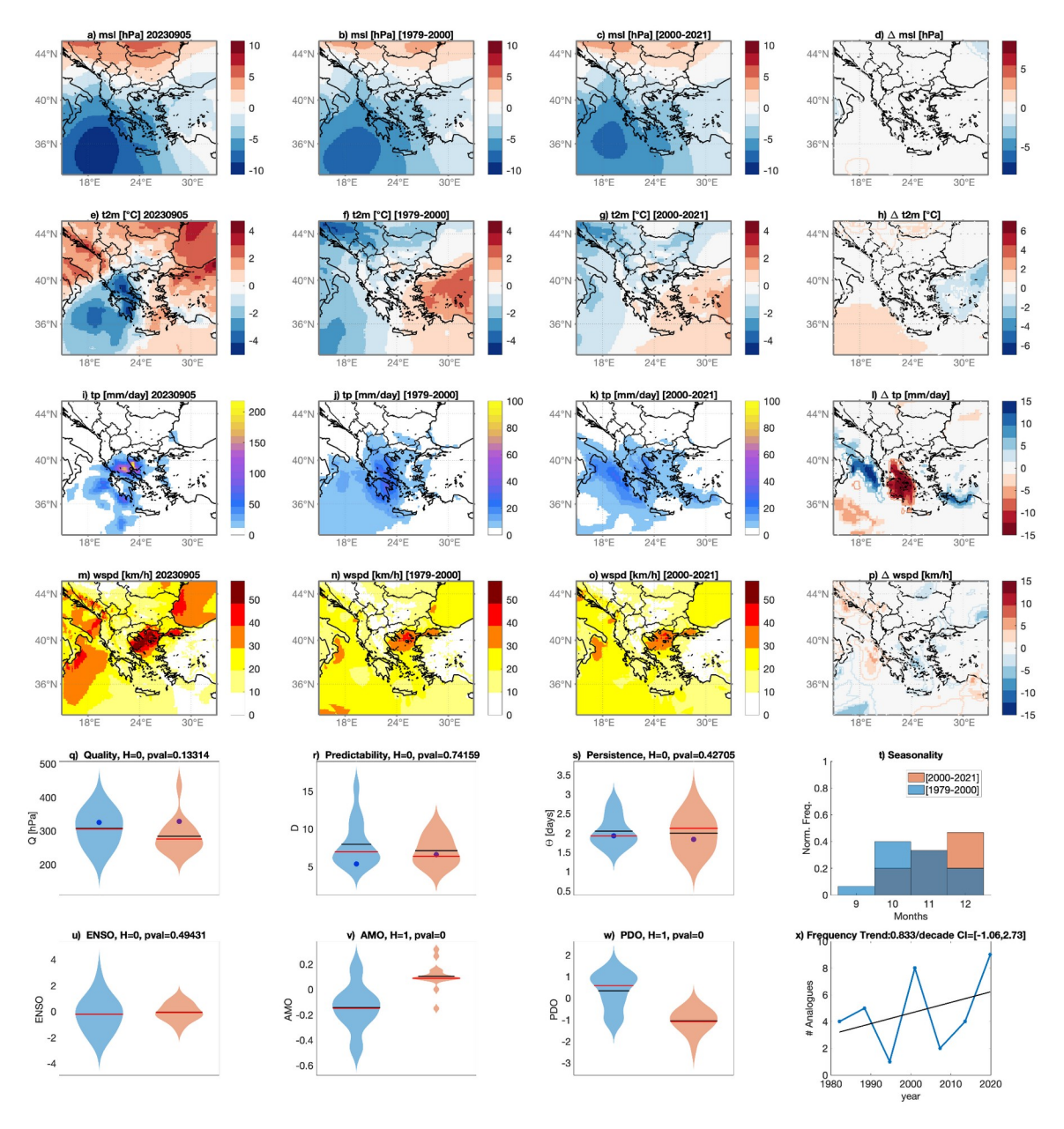


Figure 12: Analogues for 5 September 2023 and the region-defined by [15°E_-33°E_ 33°N_-45°N] and the extended summer season SOND: average surface pressure anomaly (msl) (a), average 2-meter temperature anomalies (t2m) (e), accumulated total precipitation (tp) (i), and average wind-speed (wspd) in the period of the event. Average of the surface pressure analogs found in the counterfactual [1979-2000] (b) and factual periods [2001-2022] (c), along with corresponding 2-meter temperatures (f, g), accumulated precipitation (j, k), and wind speed (n, o). Changes between present and past analogs are presented for surface pressure Δslp (d), 2-meter-2 meter temperatures Δt2m (h), total precipitation Δ tp (i), and windspeed Δ wspd (p): color-filled_shaded areas indicate significant anomalies obtained from concerning the bootstrap procedure. Contours indicate non-significant changes: Violin plots for past (blue) and present (orange) periods for Quality Q analogs (q), Predictability Index D (r), Persistence Index Θ (s), and distribution of analogs in each month (t). Violin plots for past (blue) and present (orange) periods for ENSO (u), AMO (v) and PDO (w). Number of the Analogues occurring in each subperiod (blue) and linear trend (black). A blue dot marks values for the peak day of the extreme event. Horizontal bars in panels (q,r,s,u,v,w) correspond to the mean (black) and median (red) of the distributions.

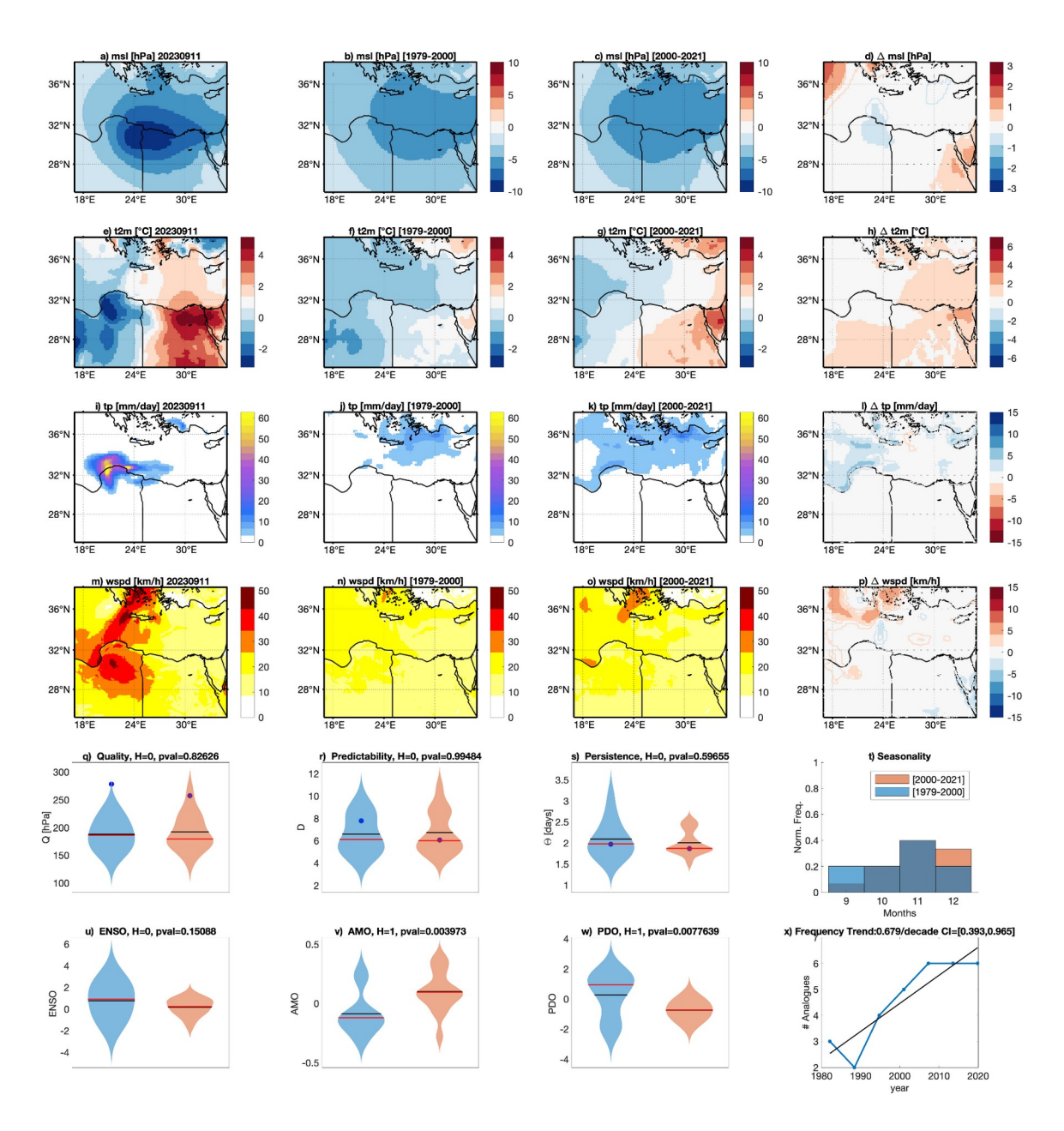


Figure 13: As in Fig. 12, but for 10-11 <u>September /09/</u>2023, the region [17°E_-35°E, 25°N_-38°N] and the extended autumn season (SOND).

1499